Classification. BIOLOGICAL SCIENCES: Medical Sciences

Title

The obesity-associated gene *TMEM18* has a role in the central control of appetite and body weight regulation

Short Title

Effect of TMEM18 on the central control of appetite

Rachel Larder[1], M. F. Michelle Sim[1], Pawan Gulati[1], Robin Antrobus[2], Y.C. Loraine Tung[1], Debra Rimmington[1], Eduard Ayuso[3], Joseph Polex-Wolf[1], Brian Y.H. Lam[1], Cristina Dias[4], Darren W. Logan[4], Sam Virtue[1], Fatima Bosch[3], Giles S.H. Yeo[1], Vladimir Saudek[1], Stephen O'Rahilly[1¥] and Anthony P. Coll[1¥]

Affiliations [1] University of Cambridge Metabolic Research Laboratories, Level 4, Wellcome Trust-MRC Institute of Metabolic Science, Box 289, Addenbrooke's Hospital, Cambridge, CB2 0QQ. United Kingdom; [2] Cambridge Institute for Medical Research, University of Cambridge, United Kingdom; [3] Center of Animal Biotechnology and Gene Therapy and Department of Biochemistry and Molecular Biology, School of Veterinary Medicine, Universitat Autònoma de Barcelona, 08193-Bellaterra and Centro de Investigación Biomédica en Red de Diabetes y Enfermedades Metabólicas Asociadas (CIBERDEM), Spain; [4] Wellcome Trust Sanger Institute, Wellcome Genome Campus, Hinxton-Cambridge, CB10 1SA, United Kingdom.

¥ **Corresponding authors**

Dr Anthony P Coll and Prof Stephen O'Rahilly
University of Cambridge Metabolic Research Laboratories
MRC Metabolic Diseases Unit
Level 4, Wellcome Trust-MRC Institute of Metabolic Science
Box 289, Addenbrooke's Hospital
Cambridge CB2 0QQ, UK
APC phone +44 1223 769041 **e-mail** apc36@cam.ac.uk
SOR phone +44 1223 336855 **e-mail** so104@medschl.cam.ac.uk

Keywords

GWAS, obesity, TMEM18, hypothalamus

Abstract

An intergenic region of human Chromosome 2 (2p25.3) harbours genetic variants which are among those most strongly and reproducibly associated with obesity. The gene closest to these variants is *TMEM18*, although the molecular mechanisms mediating these effects remain entirely unknown. *Tmem18* expression in the murine hypothalamic paraventricular nucleus (PVN) was altered by changes in nutritional state. Germline loss of *Tmem18* in mice resulted in increased body weight, which was exacerbated by high fat diet and driven by increased food intake. Selective overexpression of *Tmem18* in the PVN of wild-type mice reduced food intake and also increased energy expenditure. We provide new evidence that TMEM18 has four, not three, transmembrane domains and that it physically interacts with key components of the nuclear pore complex. Our data support the hypothesis that *TMEM18* itself, acting within the central nervous system, is a plausible mediator of the impact of adjacent genetic variation on human adiposity.

Significance statement

The growing size and sophistication of genome wide association studies has led to the identification of variants which are clearly and reliably associated with obesity. A strong association between increased BMI and a region of human chromosome 2, near to the gene *TMEM18*, has been repeatedly demonstrated in children and adults. The function of TMEM18 in the control of appetitive behaviour and body composition has been poorly characterised. In murine models, we show germline loss results in weight gain while adult onset hypothalamic overexpression results in weight loss, supporting the hypothesis that TMEM18 acting within the central nervous system can affect energy balance. We also report a novel structure and putative molecular function of TMEM18, challenging the current published model.

\body

INTRODUCTION

The understanding of human obesity has benefited greatly from advances in molecular genetics. In addition to the identification of many mechanistically illuminating, highly penetrant monogenic disorders, genome-wide association studies (GWAS) have identified multiple common genetic variants strongly associated with body mass index (BMI) (1-5). Many of these loci are within, or close to, genes which, to date, have not been recognised to encode proteins with a role in the control of energy homeostasis. Of note, these genes show a strong preponderance to being highly expressed in the central nervous system, a finding which is congruent with the fact that monogenic disorders leading to obesity largely exert their effects through a disruption of the central control of appetite and energy balance (6). Murine models have proven to be highly useful in bridging the gap between the identification of a variant as being associated with an adiposity phenotype and the understanding of how that variant actually influences energy balance. For example, the robust correlation between BMI and polymorphisms in the first intron of the human fat mass and obesity-associated (*FTO*) gene has been followed by loss and gain of function studies in genetically modified mice supporting the notion that a number of neighbouring genes including *IRX3* (which is the gene most likely mediating the effect of the human SNP), *RPGRIP1L* and *FTO* itself can all play a role in the control of energy balance and body composition (7-13). A strong association between increased BMI and a region of human chromosome 2, near to the gene *TMEM18*, has been repeatedly demonstrated in both adults and children (2, 14-18). Like the genes in the vicinity of *FTO, TMEM18* had not been recognised as having a role in energy homeostasis prior to its identification by GWAS and relatively little is known about its function, save that it is expressed in the brain and that it encodes a 140 amino acid protein reported to contain three transmembrane domain (19) which may act as a DNA-binding protein (20). We have therefore undertaken a range of studies to determine whether TMEM18 plays a role in the control of energy balance in mammals.

RESULTS

***Tmem18* is expressed within hypothalamic paraventricular nucleus.** We initially examined the expression pattern of *Tmem18* in a range of murine tissues and two mouse hypothalamic cell lines (N-46 and GT1-7). In keeping with previous reports (19), *Tmem18* was widely expressed, with expression observed in several regions of the brain, in brown adipose tissue and in both hypothalamic cell lines

(Fig. S1). We undertook qPCR analysis on hypothalamic tissue acquired by laser capture microscopy (LCM) from 3 groups of wild type mice (*ad libitum* fed, 48 hr fasted and fasted for 48 hrs with leptin administered throughout the fast). 48 hr fasting decreased PVN *Tmem18* expression by 70%, with leptin administration during the fast restoring expression back to fed levels (Fig. 1). To examine expression of *Tmem18* in other hypothalamic nuclei and also to determine expression of the three genes vicinal to *Tmem18* (*Sh3yl1*, *Snth2* and *Acp1*), in a further set of wild type animals (either *ad libitum* fed or fasted for 24hrs) we undertook RNA Seq analysis of LCM-acquired tissue from four hypothalamic nuclei (arcuate, ventral medial, paraventricular and dorsal medial nuclei) (GEO accession number GSE96627, Fig. S2). *Tmem18* expression was observed in all nuclei examined. (Fig. S3). Of note, in this data set of 24 hr fasting *vs* fed, none of the changes in expression of *Tmem18*, *Sh3yl1*, *Snth2* or *Acp1* reached statistical significance in any of the four nuclei studied (Fig. S4).

Loss of *Tmem18* expression results in an increase in body mass. Knockout mice carrying mutant allele *Tmem18*$^{tm1a(EUCOMM)Wtsi}$ (abbreviated to "*Tmem18*^{tm1a}") were generated on a C57BL/6 genetic background as part of the European Conditional Mouse Mutagenesis Program (EUCOMM) (21). The introduction of the allele results in targeted disruption of exon 2 of *Tmem18*. Q-RT-PCR analysis revealed a very low level of residual *Tmem18* transcript within the hypothalamus of homozygous mice (2.1% ±1.4), whilst heterozygous mice demonstrated a 50% decrease in transcript expression compared to *Tmem18*$^{+/+}$ (49% ±9) (Fig. S5*A*). *Tmem18* was the only transcript at that locus to be altered by introduction of the allele (Fig. S5*B*) suggesting that there were no local 'off target' effects. The mice were viable with expected homozygous mutant offspring born from heterozygous crosses. Female *Tmem18*^{tm1a} homozygotes showed no differences in body weight or body composition compared to wildtype littermates (Fig.S6*A*, *C* and *E*). Male *Tmem18*^{tm1a} homozygotes, on normal chow, had significantly increased body weight by 14 weeks of age (Fig. 2A) due to a significant increase in both fat and lean mass (Fig. 2C). At 16 weeks, male homozygotes weighed on average 1.9 g more than wildtype littermates and had both increased gonadal white adipose tissue (gWAT) and brown adipose tissue (BAT) mass (Fig. S7*A*).

Male *Tmem18* deficient mice fed a high fat diet become more obese because of an increase in food intake. To determine the effects of a high fat diet on weight gain in *Tmem18* deficient mice, WT and homozygous *Tmem18*^{tm1a} mice were switched from normal chow to a 45% fat diet (HFD) at 8 weeks of age. Female *Tmem18*^{tm1a} homozygotes on a HFD showed no differences in body weight or body composition compared to wildtype littermates (Fig. S6*B*, *D* and *F*). However, male *Tmem18*^{tm1a} homozygotes on a HFD displayed significantly increased body weight by 12 weeks of age (Fig. 2*B*) with an increase in both fat and lean mass (Fig. 2*D*). By 16 weeks of age male homozygotes on a HFD weighed ~4.1 g heavier than wildtype littermates and had both increased gWAT and BAT (Fig. S7*B*). Food intake in these mice was assessed on two occasions, firstly over a 10-day period at 15 weeks of age whilst individually housed in home cages (Fig. 3*A*), and secondly over the 72hr period at 16 weeks of ages when mice were being analyzed for energy expenditure (Fig. 3*B*). On both occasions, *Tmem18* deficient mice consumed significantly more energy than wildtype littermates. Interestingly, at the time of indirect calorimetry, *Tmem18* deficient males on HFD had a significantly increased energy expenditure compared to wildtype littermates (ANCOVA analysis with correction for body weight differences, *p=0.015, Figs. 3*C* and 3*D*). Between genotypes, there was no difference in the expression of markers of thermogenesis in brown adipose tissue (Fig. S8*A*) or in activity levels (Fig. S8*B*). Thus, the increase in food intake (13.9%) in animals lacking *Tmem18* was partially compensated for by a rise in energy expenditure (7.0%), resulting in only a modest increase in weight.

Overexpression of *Tmem18* within the PVN reduces food intake and increases energy expenditure. Having determined that *Tmem18* expression in the PVN was altered by changes in nutritional state, we used adeno-associated viral vector (AAV-T18) to manipulate expression of *Tmem18* within the PVN and study subsequent effect on feeding behaviour and body weight. Having confirmed targeting studies using AAV over-expressing GFP (Fig. S9*A*), we then performed bilateral injections of an AAV-*Tmem18*-cDNA into the PVN of 12 week old C57/BL6 male mice. Compared to control mice, mice who received vectors expressing *Tmem18* cDNA had a significant two-fold increase in expression level (Fig. 4*A*). We found a significant difference in body weight gain at 2 weeks post-surgery and by 6 weeks, mean weight gain in mice overexpressing *Tmem18* was only 0.9 g compared to a 2.7 g in the control group (absolute weight gain; Fig. 4*B*: percentage weight gain; Fig. 4*C*). Analysis of food intake

at 2 weeks post-surgery demonstrated AAV-T18 treated mice to have a significant reduction in food intake which was likely to have contributed to their reduction in weight gain (Fig. 4*D*). Interestingly, when re-assessed at 6 weeks, this relative hypophagia appeared to have resolved with no difference in energy intake between genotypes (Fig. 4*E*). However, at 6 weeks post-surgery there was a significant difference in energy expenditure with AAV-T18 treated mice showing an increase compared to the control group (Fig. 4*F*, ANCOVA analysis with correction for body weight differences, *p=0.03).Additionally, a separate group of mice (n=6) over-expressing *Tmem18* were placed on a high fat diet immediately after stereotactic surgery. Again, mice over-expressing *Tmem18* gained significantly less weight (Fig. S9*D*). There was a trend for a reduction in energy intake at 2 weeks (Fig. S9*E*) and at 6 weeks there was a significant difference in both total and fat mass between groups (Fig. S9*F*).

TMEM18 contains four, not three, transmembrane domains TMEM18 has been described to be a three transmembrane protein that localizes to the nuclear membrane, courtesy of a nuclear localization signal, and reported to be involved in transcriptional repression (19, 20). To test this hypothesis, we first embarked on a deep phylogenetic analysis exploring sequence profile-to-profile homology (22) with MPI Bioinformatics Toolkit software (23). Database searches revealed remote but clear homology of TMEM18 to various ion channels. These included proteins from Pfam families (http://pfam.xfam.org) of fungal transient receptor potential ion channels (PF06011) and bacterial mechanosensitive ion channels (PF12794). Searches in metazoan proteomes yielded Unc-93 A homologues (mammalian gene UNC93A) annotated in *C. elegans* as an ion channel. The top hits (Toolkit parameter of probability of true positives about 80%) comprised a voltage-gated sodium channel from *Caldalkalibacillus thermarum* and an ion transport protein from *Arcobacter butzleri* (PDB identifiers 4bgn and 3rvy). Although their mutual phylogenetic distances are remote, they fold into a very similar structure and TMEM18 shares suggestive homology with their ion-transmitting domain. This region forms an oligomer consisting of two N- and C-terminal transmembrane helices pointing to the cytoplasm and two shorter inner helices fully embedded in the membrane. The conserved charged tip of their C-terminal helices is entirely outside the membrane and participates in the pore opening. It is highly probable that TMEM18 possesses a very similar topology and structure. Based on the homology to the *C. thermarum* channel, a tentative model can be proposed. Fig. S10 shows the modelled membrane topology and a putative 3D structure under the assumption that TMEM18 forms

a tetramer similar to the *A. butzleri* channel (24). As a nuclear membrane protein, it should expose both its termini to the cytoplasm and therefore would be comprised of four, rather than three, transmembrane domains. To test this experimentally we transfected Cos cells with a N-terminal FLAG-tagged *Tmem18* construct then detected protein expression using either a FLAG antibody or a TMEM18 antibody raised against C-terminus amino acids 120-134. Protein expression was analyzed using two different detergents, TX100 that permeabilises all cellular membranes and digitonin, that only permeabilises the plasma membrane at a concentration of 40ug/ml. Control antibodies (lamin B and calnexin) gave the expected results. Lamin B, which is localized to the inside of the nuclear membrane could only be detected when TX100 was used to permeabilise both the plasma and nuclear membrane (Fig. S11*A* & *B*) whereas calnexin, which spans the nuclear membrane with the C-terminus pointing into the cytoplasm, could be detected with both permeabilisation reagents using a C-terminal antibody (Fig. S11*C* & *D*). Both the N-terminus (FLAG antibody, Fig. 5*A* & 5*B*) and C-terminus (TMEM18 antibody, Fig. 5*C* & 5*D*) of TMEM18 could be detected with digitonin permeabilisation indicating that both ends of the protein were located within the cytoplasm and confirming the bioinformatics analysis which suggested that TMEM18 is a four transmembrane protein.

TMEM18 is unlikely to directly regulate transcription It has been suggested that TMEM18 binds DNA and supresses transcription (20). To test this hypothesis, we performed RNA-Seq analysis of hypothalami from wildtype and *Tmem18* knockout male mice (ENA accession PRJEB13884). Altogether, 27691 (27727 with non-zero total read count; 36 outliers per cooks Cutoff (25)) annotated genes had reads mapped in at least one sample and were used for differential expression analysis (average number of uniquely mapped reads per sample: 32.4x10-6 ± 2.04x10-6 SD). Interestingly, after adjustment for multiple testing, only *Tmem18* was significantly differentially expressed within the hypothalami of the two genotypes (padj = 3.02 x 10-22, Fig. S12*A*). Q RT PCR analysis of *Tmem18* and six additional genes with smallest (but not statistically significant) padj values confirmed the RNAseq data (Fig. S12*B*), suggesting that TMEM18 is unlikely to be a global regulator of transcription as previously reported (20).

TMEM18 interacts with two nuclear pore proteins, NDC1 and AAAS We used the methods of affinity purification and mass spectrometry (26) to identify novel TMEM18 interacting partners. Either FLAG-tagged TMEM18 or empty FLAG vector were over expressed in HEK293 cells. Protein complexes were immunoprecipitated using a FLAG antibody and mass

spectrometry analysis performed to detect proteins bound to TMEM18. This process identified 116 proteins pulled down in control cells expressing the empty FLAG vector, 221 proteins common to both the control and experimental group, and 244 proteins unique to cells expressing FLAG-TMEM18 (See Supplementary Table 1 for a list of all proteins identified as being pulled down by FLAG-TMEM18). Interestingly, three members of the nuclear pore complex, NDC1, AAAS and NUP35/53 (27) showed high numbers of assigned spectra indicating a high abundance of these proteins after pulldown. Therefore, biomolecular immunofluorescence complementation (BiFC) assays were employed to confirm interactions between these proteins and TMEM18. Controls behaved as expected and showed that no YFP expression was seen if YN constructs were co-transfected with a YC-STOP plasmid (Fig. 6*A*). YN-FLAG-NDC1 and YC-AAAS served as an appropriate positive control (Fig. 6*B*) as these proteins have been reported to interact previously (28, 29). YFP expression could be detected in cells expressing YC-TMEM18 and either YN-FLAG-NDC1 or YN-FLAG-AAAS; but not YN-FLAG-NUP35 (Fig. 6*C*-*G*). Positive BiFC protein-protein interactions were corroborated further by co-immunoprecipitation experiments using FLAG-TMEM18 and either GFP tagged NDC1 (Fig. 6*H*) or GFP tagged AAAS (Fig. 7*I*).

DISCUSSION

Our data indicate that altering *Tmem18* expression in mice, both globally and within the hypothalamus, can alter body weight. Male mice with a germline loss of *Tmem18* have an increased body weight due to a significant increase in both fat and lean mass. This phenotype is more pronounced on a high fat diet, where weight gain is driven by hyperphagia. In contrast, overexpression of *Tmem18* expression within the hypothalamic PVN can reduce food intake, increase energy expenditure and reduce both total body and fat mass. The increased body weight phenotype of *Tmem18* null mice was sexually dimorphic. Sex-specific differences in metabolic studies focusing on body weight are not uncommon and have been seen, for example, after embryonic TrkB inhibition or with disruption of GABA receptor signalling in proopiomelanocortin neurons (30, 31). In these reports and in our current study data, the mechanisms behind the sex-specific changes in body weight remain to be fully determined but the differences in circulating gonadal derived hormones remain, of course, a potential contributor. Indeed, the relevance of oestrogen in influencing the response to a dietary intervention was highlighted again in a study by Dakin *et. al.* in which oestradiol

treatment to male mice fed a high-fat, high-sugar 'obesogenic' diet prevented increases in adipose tissue mass (32).

Male mice on a high fat diet gained weight because of increased energy intake. Of note, data from indirect calorimetry also showed *Tmem18* null mice to have a ~10% increase in energy expenditure compared to wild type mice, but as food intake was increased by ~30% the dominant drive was to caloric excess and weight gain. This could be considered an example of "diet induced thermogenesis", a state seen as an effect of a change to a higher calorie diet in which mice increase energy expenditure and food intake simultaneously (33). The potential biological purpose and the tissues relevant to this phenomenon continue to be disputed (34). There is more agreement that the ambient temperature of a study can have a strongly qualitative effect on the outcome of metabolic studies (35). Our studies were conducted under "standard" animal house conditions that could be considered a chronic thermal stress to mice. Future studies of energy expenditure in *Tmem18* deficient mice living at thermoneutrality may be helpful in further understanding the role of this molecule in metabolic control.

Several groups have previously shown *Tmem18* to be highly expressed within the hypothalamus, although not all have reported it to be nutritionally regulated (19, 36, 37). Our data also indicate that *Tmem18* is expressed within a number of hypothalamic regions. We chose to focus on the PVN, an anatomical region enriched with neuronal populations involved in appetitive behaviour and energy expenditure (38) and one in which we saw nutritional regulation. The character of *Tmem18* expressing neurons within the PVN remain to be determined. Further, the nature of the different perturbations (germline loss in *Tmem18*^{tm1a} *vs* delivery of AAV via stereotactic injection) is likely to mean that the PVN neuronal population which lost *Tmem18* expression in the null mice may not be the same population that gained overexpression in the stereotactic-driven AAV study. We were unfortunately unsuccessful in our attempts to use siRNA and *Cre* to selectively knock down and/or delete *Tmem18* in the PVN despite promising preliminary studies *in vitro*. In the future, transgenic lines with specific anatomical *Cre* drivers (e.g. *Sim1-Cre*, *Agrp-Cre*) may be helpful to further delineate the role of TMEM18 in both hypothalamic nuclei and specific neuronal populations.

We report interesting new data on the potential function of TMEM18. Previous reports have indicated that TMEM18 is highly conserved, has no family members, localizes at the nuclear membrane and that the C-terminus of the protein may be involved in the regulation of

transcription. Whilst the localization of TMEM18 is not disputed we propose that a role for TMEM18 in transcriptional regulation is unlikely given our RNA-Seq data showing that the hypothalamic transcriptome of *Tmem18*^{tm1a} mice is not significantly different to that of wildtype littermates. Previous bioinformatic analysis had predicted a 3 transmembrane structure (19, 39). However, our cellular experiments reveal that TMEM18 is in fact comprised of four transmembrane segments indicating that it is unlikely that the C-terminus is involved in binding DNA as earlier reported (20). Instead we hypothesise that TMEM18 may be involved in the transport of molecules across the nuclear envelope. Pull-down experiments, corroborated by BiFC and IP studies have identified two novel binding partners for TMEM18 – NDC1 and AAAS/ALADIN. These proteins are two of the thirty NUPs that make up the nuclear pore complex (NPC) (40). As NDC1 and AAAS have previously been reported to interact with one another (29) it is possible that TMEM18 is not interacting directly with both proteins. By enabling transport of molecules across the nuclear envelope, NUPs are involved in many fundamental cellular processes, consequently abnormal expression/function of these NUPs has been linked to various human diseases such as cancer, cardiovascular disorders, autoimmune disease and neurological defects (41). Further investigation into the interaction of TMEM18 with members of the NPC will hopefully shed new light on the molecular function of TMEM18 and its role in obesity.

The association of single nucleotide polymorphisms (SNPs) near human *TMEM18* with obesity was first reported by Willer *et al.* (2) and has since been identified by multiple GWAS (reviewed in (6)). Although these loci have taken on the moniker of 'near to *TMEM18*', to date it has remained unclear whether these variants have any influence on the regulation of *TMEM18* expression or function, or indeed if TMEM18 has a direct role in energy homeostasis. Efforts to advance understanding from association to biologically relevant mechanisms have combined multiple techniques and evidence from several model platforms. For example, when investigating obesity-associated noncoding sequences within *FTO*, Smemo used chromatin conformation capture techniques (CCST) to show a region of *FTO* directly interacts with, and forms part of the regulatory landscape of, the homeobox gene *IRX3* (10). They also reported that relevant SNPS were associated with expression of *IRX3*, but not *FTO*, in human brains. In a more recent study of obesity associated *FTO* variants, Claussnitzer combined chromatin capture technology, eQTL data and a powerful bioinformatics approach to investigate a putative role for FTO adipocyte biology (42). Thus far our attempts to interrogate

the region near *TMEM18* through the examination of various gene expression databases shows no eQTL data relevant to these SNPs. Further, our data are insufficient to confirm or refute a role for other genes vicinal to *TMEM18* as candidates of the GWAS association. A brain tissue specific approach may prove more fruitful but unfortunately RNA expression data specifically from human hypothalamus linked to genotype is not a currently publicly available resource. The studies we have described have strengthened the candidacy of *TMEM18* as, at least in part, the mediator of the association between genetic variation in this region of chromosome 2 and human adiposity, one of the strongest associations of a common variant with human obesity. Our work has also provided novel information about the topology and binding partners of this enigmatic protein associated with the nuclear pore complex.

METHODS

Detailed study methods are provided in SI appendix

Animals. All procedures were carried out in accordance with guidelines of the United Kingdom Home Office. Animals were kept under controlled temperature (22^{o}C) and a 12-h light, 12-h dark schedule (lights on 7:00–19:00).

AAV Vectors*.* The cDNA of murine *Tmem18* was cloned into an AAV backbone plasmid under the control of the CMV promoter. AAV vectors were generated by helper virus-free transfection of HEK293 cells.

Stereotactic surgery*.* Mice were stereotaxically injected with AAV while under isoflurane induced anaesthesia (coordinates; 1.0 mm caudal to bregma, ±0.25 mm lateral to the midline, 5.0 mm below the surface of the skull).

Metabolic phenotyping. Body composition was determined using Lunar PIXImus2 mouse densitometer (General Electric Medical Systems, Fitchburg, WI).Energy expenditure was determined using indirect calorimetry in a custom built monitoring system (Ideas Studio, Cambridge, UK).

Laser capture microdissection Coronal sections of 20 um thickness were prepared on a cryostat, mounted on RNase-free membrane-coated glass slides with laser microdissection performed using a P.A.L.M. MicrolaserSystem (P.A.L.M. Microlaser Technologies).

Pulldown and Mass Spec analysis*.* For protein over expression studies, transient transfection in HEK293 cells was performed using a CalPhos kit according to the manufacturer's protocol. 48 hours post transfection, cells were harvested and Flag immunoprecipitations (IPs) were performed from the resulting lysates.

Statistical Analysis*.* All values are expressed as mean ±S.E.M. Statistical analysis was performed using Graph Pad Prism software (GraphPad Prism) or SPSS (IBM). For the analysis of food intake and body weight over time, two-way repeated measures ANOVA, with a Bonferroni post-test, was used with time and treatment as variables for comparison. For energy expenditure (EE) analysis of covariance (ANCOVA) was performed to assess body weight/EE interactions with body weight as a covariate, genotype or AAV treatment as a fixed factor and EE as a dependent variable. Multiple linear regression analysis was carried out with no selection criteria. Differential expression in LCM tissue analysis was calculated using

edgeR, with correction for multiple comparisons using the Benjamini-Hochberg procedure. Significant differences were designated as $p < 0.05$.

AUTHOR CONTRIBUTIONS

RL, MS, LT, DR, PG, RA, SV, VS, GY and APC conducted the experiments and/or analysed data. JPW and BL conducted and analysed all RNA Seq experiments on fed and fasted wild-type mice. EA and FB produced and purified viral vectors. CD and DWL conducted and analysed all RNA Seq experiments on *Tmem18* knockout tissue. RL, GY, SO'R and APC designed the experiments. RL, SO'R and APC wrote the manuscript.

ACKNOWLEDGEMENTS

The authors thank Helen Westby, Will Gee and Elizabeth Wynn for technical assistance. We also thank Satish Patel and Koini Lim for assistance with the BiFC protocol. RL, YCLT, DR, GSHY, SOR and APC are funded by the Medical Research Council (MRC) Metabolic Disease Unit (MRC_MC_UU_12012/1) and animal work was carried out with the assistance of MRC Disease Model Core of the Wellcome Trust MRC Institute of Metabolic Sciences (MRC_MC_UU_12012/5 and Wellcome Trust Strategic Award (100574/Z/12/Z). F. Bosch is the recipient of an award from the ICREA Academia, Generalitat de Catalunya, Spain. Vector generation and production were funded by Ministerio de Economía y Competitividad (SAF 2014-54866-R), Spain. CD and DWL were supported by the Wellcome Trust (WT098051) and CD was supported by the Wellcome Trust PhD Programme for Clinicians (100679/Z/12/Z).

REFERENCES

1. Frayling TM*, et al.* (2007) A common variant in the FTO gene is associated with body mass index and predisposes to childhood and adult obesity. *Science* 316(5826):889-894.
2. Willer CJ*, et al.* (2009) Six new loci associated with body mass index highlight a neuronal influence on body weight regulation. *Nat Genet* 41(1):25-34.
3. Speliotes EK*, et al.* (2010) Association analyses of 249,796 individuals reveal 18 new loci associated with body mass index. *Nat Genet* 42(11):937-948.
4. Thorleifsson G*, et al.* (2009) Genome-wide association yields new sequence variants at seven loci that associate with measures of obesity. *Nat Genet* 41(1):18-24.
5. Meyre D*, et al.* (2009) Genome-wide association study for early-onset and morbid adult obesity identifies three new risk loci in European populations. *Nat Genet* 41(2):157-159.
6. Loos RJ (2012) Genetic determinants of common obesity and their value in prediction. *Best Pract Res Clin Endocrinol Metab* 26(2):211-226.
7. Church C*, et al.* (2010) Overexpression of Fto leads to increased food intake and results in obesity. *Nat Genet* 42(12):1086-1092.
8. Fischer J*, et al.* (2009) Inactivation of the Fto gene protects from obesity. *Nature* 458(7240):894-898.
9. McMurray F*, et al.* (2013) Adult onset global loss of the fto gene alters body composition and metabolism in the mouse. *PLoS Genet* 9(1):e1003166.
10. Smemo S*, et al.* (2014) Obesity-associated variants within FTO form long-range functional connections with IRX3. *Nature* 507(7492):371-375.
11. Stratigopoulos G*, et al.* (2016) Hypomorphism of Fto and Rpgrip1l causes obesity in mice. *The Journal of clinical investigation*.
12. Tung YC*, et al.* (2010) Hypothalamic-specific manipulation of Fto, the ortholog of the human obesity gene FTO, affects food intake in rats. *PLoS One* 5(1):e8771.
13. Stratigopoulos G*, et al.* (2014) Hypomorphism for RPGRIP1L, a ciliary gene vicinal to the FTO locus, causes increased adiposity in mice. *Cell Metab* 19(5):767-779.
14. Felix JF*, et al.* (2016) Genome-wide association analysis identifies three new susceptibility loci for childhood body mass index. *Human molecular genetics* 25(2):389-403.
15. Pei YF*, et al.* (2014) Meta-analysis of genome-wide association data identifies novel susceptibility loci for obesity. *Human molecular genetics* 23(3):820-830.
16. Scherag A*, et al.* (2010) Two new Loci for body-weight regulation identified in a joint analysis of genome-wide association studies for early-onset extreme obesity in French and german study groups. *PLoS Genet* 6(4):e1000916.
17. Paternoster L*, et al.* (2011) Genome-wide population-based association study of extremely overweight young adults--the GOYA study. *PLoS One* 6(9):e24303.
18. Zhao J*, et al.* (2011) Role of BMI-associated loci identified in GWAS meta-analyses in the context of common childhood obesity in European Americans. *Obesity (Silver Spring)* 19(12):2436-2439.
19. Almen MS*, et al.* (2010) The obesity gene, TMEM18, is of ancient origin, found in majority of neuronal cells in all major brain regions and associated with obesity in severely obese children. *BMC Med Genet* 11:58.
20. Jurvansuu JM & Goldman A (2011) Obesity risk gene TMEM18 encodes a sequence-specific DNA-binding protein. *PLoS One* 6(9):e25317.
21. Skarnes WC*, et al.* (2011) A conditional knockout resource for the genome-wide study of mouse gene function. *Nature* 474(7351):337-342.
22. Soding J (2005) Protein homology detection by HMM-HMM comparison. *Bioinformatics* 21(7):951-960.

23. Alva V, Nam SZ, Soding J, & Lupas AN (2016) The MPI bioinformatics Toolkit as an integrative platform for advanced protein sequence and structure analysis. *Nucleic Acids Res* 44(W1):W410-415.
24. Tsai CJ*, et al.* (2013) Two alternative conformations of a voltage-gated sodium channel. *J Mol Biol* 425(22):4074-4088.
25. Love MI, Huber W, & Anders S (2014) Moderated estimation of fold change and dispersion for RNA-seq data with DESeq2. *Genome Biol* 15(12):550.
26. Gingras AC, Gstaiger M, Raught B, & Aebersold R (2007) Analysis of protein complexes using mass spectrometry. *Nature reviews. Molecular cell biology* 8(8):645-654.
27. Kabachinski G & Schwartz TU (2015) The nuclear pore complex--structure and function at a glance. *Journal of cell science* 128(3):423-429.
28. Kind B, Koehler K, Lorenz M, & Huebner A (2009) The nuclear pore complex protein ALADIN is anchored via NDC1 but not via POM121 and GP210 in the nuclear envelope. *Biochemical and biophysical research communications* 390(2):205-210.
29. Yamazumi Y*, et al.* (2009) The transmembrane nucleoporin NDC1 is required for targeting of ALADIN to nuclear pore complexes. *Biochemical and biophysical research communications* 389(1):100-104.
30. Byerly MS, Swanson RD, Wong GW, & Blackshaw S (2013) Stage-specific inhibition of TrkB activity leads to long-lasting and sexually dimorphic effects on body weight and hypothalamic gene expression. *PLoS One* 8(11):e80781.
31. Ito Y*, et al.* (2013) GABA type B receptor signaling in proopiomelanocortin neurons protects against obesity, insulin resistance, and hypothalamic inflammation in male mice on a high-fat diet. *J Neurosci* 33(43):17166-17173.
32. Dakin RS, Walker BR, Seckl JR, Hadoke PW, & Drake AJ (2015) Estrogens protect male mice from obesity complications and influence glucocorticoid metabolism. *Int J Obes (Lond)* 39(10):1539-1547.
33. Rothwell NJ & Stock MJ (1979) A role for brown adipose tissue in diet-induced thermogenesis. *Nature* 281(5726):31-35.
34. Kozak LP (2010) Brown fat and the myth of diet-induced thermogenesis. *Cell Metab* 11(4):263-267.
35. Feldmann HM, Golozoubova V, Cannon B, & Nedergaard J (2009) UCP1 ablation induces obesity and abolishes diet-induced thermogenesis in mice exempt from thermal stress by living at thermoneutrality. *Cell Metab* 9(2):203-209.
36. Yoganathan P, Karunakaran S, Ho MM, & Clee SM (2012) Nutritional regulation of genome-wide association obesity genes in a tissue-dependent manner. *Nutr Metab (Lond)* 9(1):65.
37. Schmid PM*, et al.* (2012) Expression of fourteen novel obesity-related genes in Zucker diabetic fatty rats. *Cardiovasc Diabetol* 11:48.
38. Cowley MA*, et al.* (1999) Integration of NPY, AGRP, and melanocortin signals in the hypothalamic paraventricular nucleus: evidence of a cellular basis for the adipostat. *Neuron* 24(1):155-163.
39. Jurvansuu J*, et al.* (2008) Transmembrane protein 18 enhances the tropism of neural stem cells for glioma cells. *Cancer Res* 68(12):4614-4622.
40. Hoelz A, Debler EW, & Blobel G (2011) The structure of the nuclear pore complex. *Annu Rev Biochem* 80:613-643.
41. Nofrini V, Di Giacomo D, & Mecucci C (2016) Nucleoporin genes in human diseases. *Eur J Hum Genet* 24(10):1388-1395.
42. Claussnitzer M*, et al.* (2015) FTO Obesity Variant Circuitry and Adipocyte Browning in Humans. *N Engl J Med* 373(10):895-907.

Figure legends

Fig. 1. *Tmem18* expression within the hypothalamic paraventricular nucleus is nutritionally regulated. Q-RT-PCR analysis showing changes in *Tmem18* gene expression in the PVN of wildtype mice that have been fed, fasted for 48hrs or fasted for 48hrs with leptin administration. Data are expressed as mean ± SEM; * p<0.05, ** p<0.01 *vs* fasted mice.

Fig. 2. Germline loss of *Tmem18* results in increased body weight in male mice. Body weights of Tmem18 $^{wt/wt}$ (WT) and Tmem18 $^{tm1a/tm1a}$ (HOM) male mice on (A) normal chow from weaning (WT, n=23; HOM, n=23) or (B) high fat diet (HFD) from 8 weeks of age (WT, n=15; HOM, n=20). Body composition analyses showing total, lean or fat mass of 14-week old WT and HOM male mice on (C) normal chow (WT, n=16; HOM, n=16) or (D) HFD from 8 weeks of age (WT, n=18; HOM, n=20). Data are expressed as mean ± SEM; * p<0.05, ** p<0.01, *** p<0.001 *vs* WT mice.

Fig. 3. Effect of loss of expression of Tmem18 on energy homeostasis, activity levels and food intake in male mice fed a HFD. Average 24-hour energy intake of WT and homozygous male mice both (A) measured in their home cage and (B) measured in the indirect calorimetry cage. (C) ANCOVA analysis of 24-hour energy expenditure (EE) with body weight at time of analysis. (D) Average bodyweight of individual animals during 72hr analysis of energy expenditure. For all panels WT n=13, HOM n=18. Data are expressed as mean ± SEM;* p<0.05, ** p<0.01 *vs* WT mice.

Fig. 4. Overexpression of *Tmem18* within the PVN. (A) Change in *Tmem18* gene expression within the PVN of mice 7 weeks after bilateral injection of an adeno-associated-vector (AAV-T18) (n= 10-11). Change in body weight of mice, measured weekly for 6 weeks after bilateral PVN injections with either an AAV-T18 cDNA or AAV-GFP (n=15 each group), expressed as grams (B) and as percentage of starting body weight (C). (D) Average 24-hour energy intake of mice, measured in their home cage, 2 weeks post-surgery (n=15 each group). (E) Average 24-hour energy intake of mice, in the indirect calorimetry cage, 6 weeks post-surgery (n=13 each group). (F) ANCOVA analysis of total energy expenditure (EE), assessed over a 24-hour period 6-weeks post injection, with covariates evaluated at body weight=29.41g (n=13 each group). Data are expressed as mean ± SEM,* p<0.05, ** p<0.01, *** p<0.001 *vs* GFP injected mice.

Fig. 5. Topology of the TMEM18 protein. (A-D) Over-expression of N-terminal FLAG-tagged TMEM18 in COS cells treated with either TX-100 (permeabilises both plasma & nuclear membrane) or digitonin (permeabilises plasma membrane only). TMEM18 expression was detected with either a FLAG antibody (red, A&B) or an antibody to the C-terminus of TMEM18 (green, C&D).

Fig. 6. BiFC and co-IP confirmation of TMEM18 interaction with NDC1 and AAAS (A-G) Physical interaction between TMEM18 and NDC1 and AAAS was confirmed by BiFC. The N-terminus of YFP was fused to FLAG-tagged NDC1 (YN-F-NDC1, panel C) or AAAS (YN-F-AAAS, panel E) or NUP35 (negative control, YN-F-NUP35, panel G), while the C-terminus of YFP was fused to TMEM18 (TMEM18-Yc). FLAG expression was detected using a FLAG antibody (red) while YFP signal is depicted in green. YN-F-NDC1 and AAAS-YC was used as a positive BiFC control (panel B). (H and I) Co-immunoprecipitation experiments using FLAG-tagged TMEM18 and GFP-tagged NDC1 (H) or AAAS (I) overexpressed in HEK cells. Dashed lines in the blot represents two different lanes in the same blot put together.

Figure 1

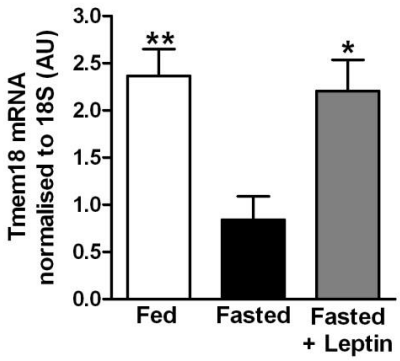
Tmem18 mRNA
normalised to 18S (AU)
3.0
2.5
2.0
1.5
1.0
0.5
0.0
**
*
Fed
Fasted
Fasted
+ Leptin

Figure 2

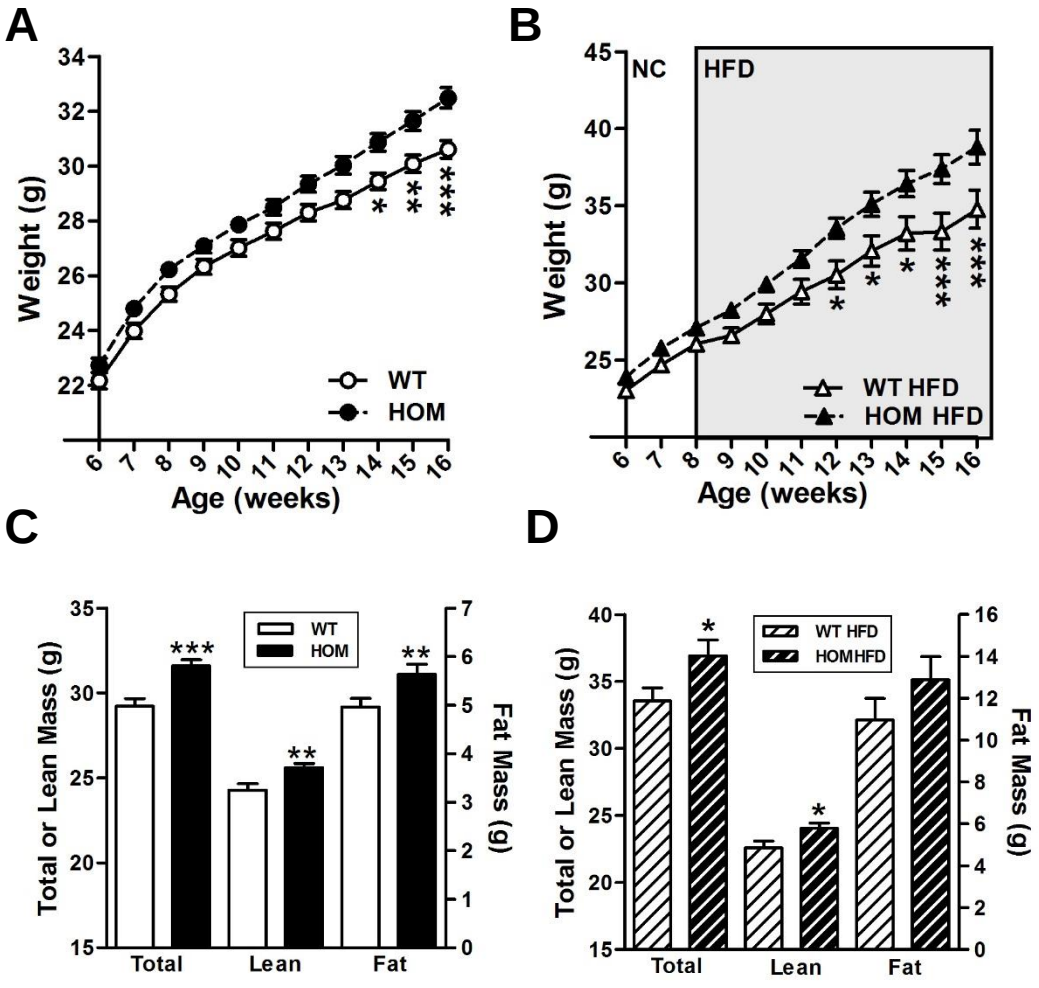
A
Weight (g)
Age (weeks)
WT
HOM
B
NC
HFD
Weight (g)
Age (weeks)
WT HFD
HOM HFD
C
Total or Lean Mass (g)
Fat Mass (g)
WT
HOM
Total
Lean
Fat
D
Total or Lean Mass (g)
Fat Mass (g)
WT HFD
HOM HFD
Total
Lean
Fat

Figure 3

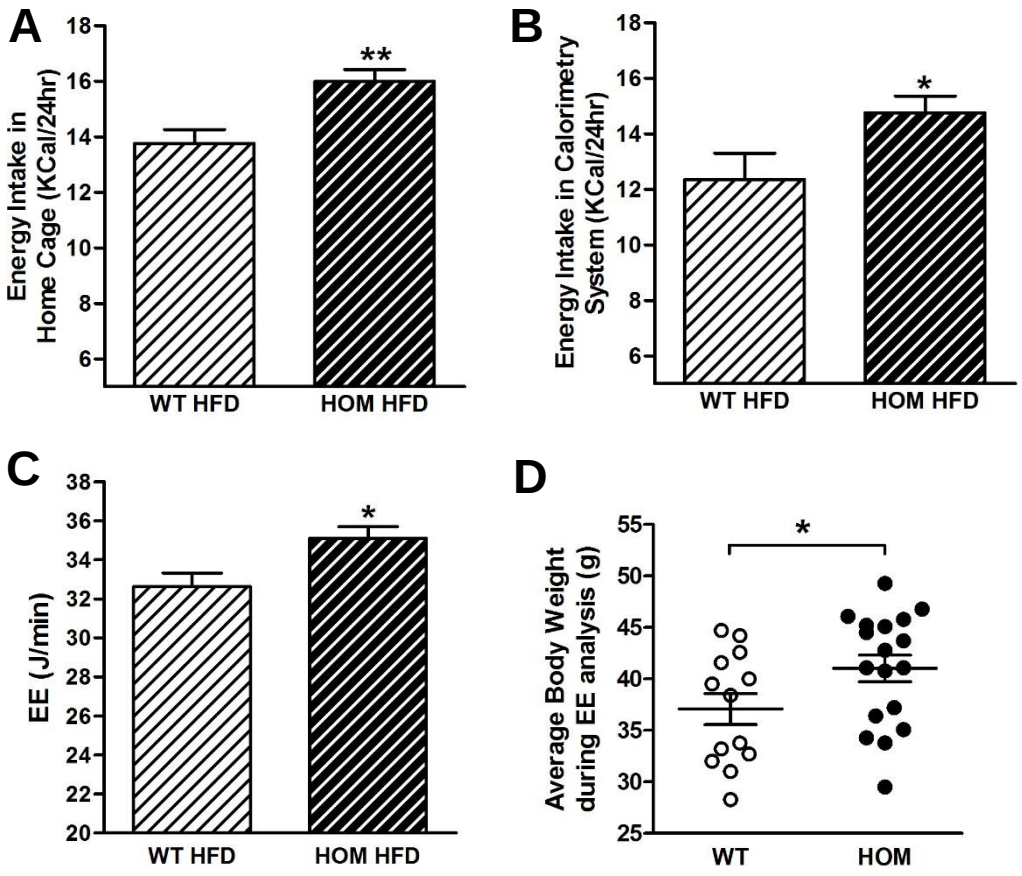
A
Energy Intake in Home Cage (KCal/24hr)
18
16
14
12
10
8
6
**
WT HFD
HOM HFD
B
Energy Intake in Calorimetry System (KCal/24hr)
18
16
14
12
10
8
6
*
WT HFD
HOM HFD
C
EE (J/min)
38
36
34
32
30
28
26
24
22
20
*
WT HFD
HOM HFD
D
Average Body Weight during EE analysis (g)
55
50
45
40
35
30
25
*
WT
HOM

Figure 4

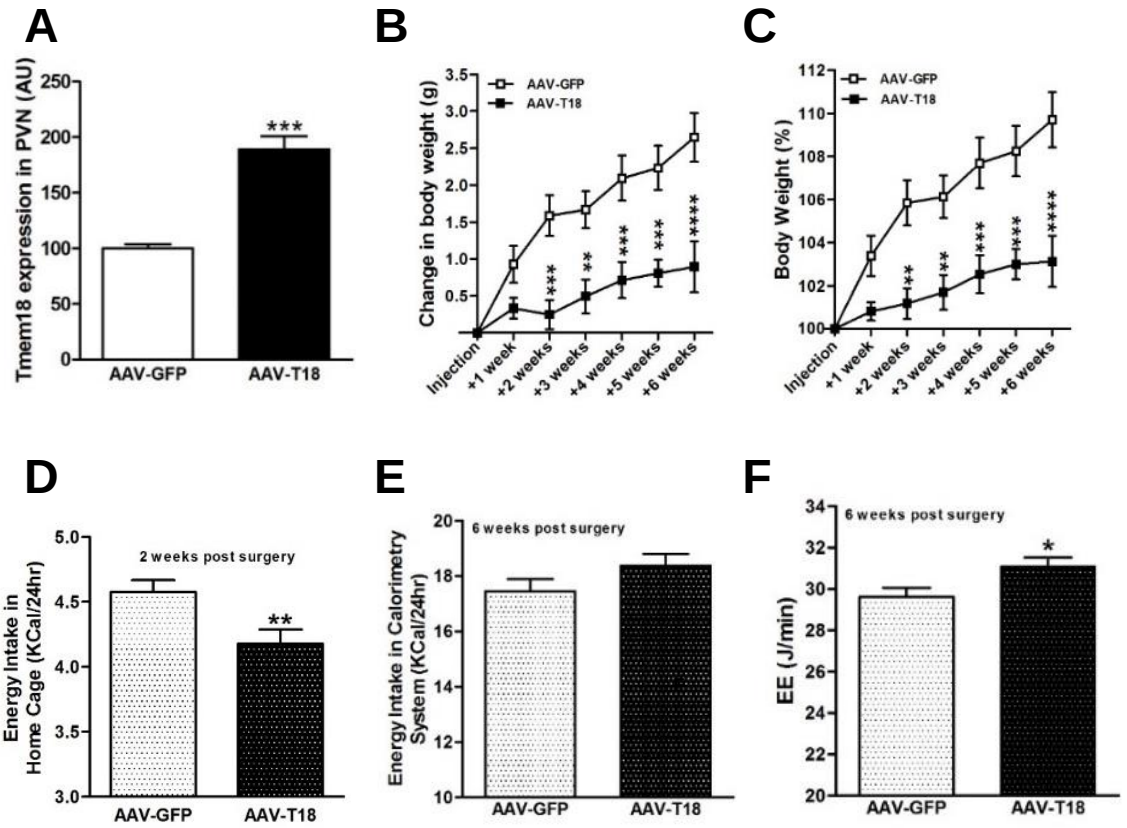
A
Tmem18 expression in PVN (AU)
250
200
150
100
50
0
***
AAV-GFP
AAV-T18
B
Change in body weight (g)
3.5
3.0
2.5
2.0
1.5
1.0
0.5
AAV-GFP
AAV-T18
***
**
***
***
****
Injection
+1 week
+2 weeks
+3 weeks
+4 weeks
+5 weeks
+6 weeks
C
Body Weight (%)
112
110
108
106
104
102
100
AAV-GFP
AAV-T18
**
***
***
*****
Injection
+1 week
+2 weeks
+3 weeks
+4 weeks
+5 weeks
+6 weeks
D
Energy Intake in Home Cage (KCal/24hr)
5.0
4.5
4.0
3.5
3.0
2 weeks post surgery
**
AAV-GFP
AAV-T18
E
Energy Intake in Calorimetry System (KCal/24hr)
20
18
16
14
12
10
6 weeks post surgery
AAV-GFP
AAV-T18
F
EE (J/min)
34
32
30
28
26
24
22
20
6 weeks post surgery
*
AAV-GFP
AAV-T18

Figure 5

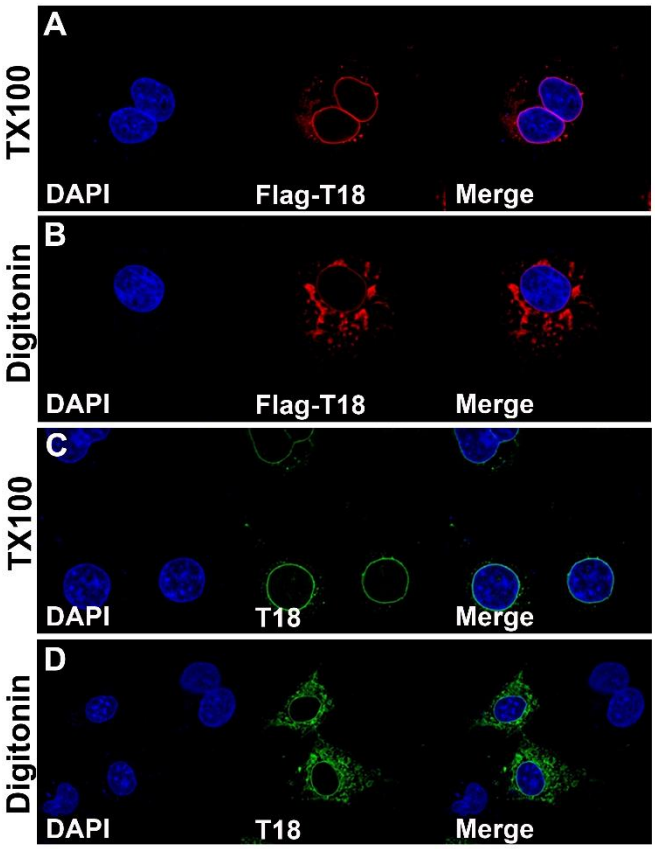
A
TX100
DAPI
Flag-T18
Merge
B
Digitonin
DAPI
Flag-T18
Merge
C
TX100
DAPI
T18
Merge
D
Digitonin
DAPI
T18
Merge

Figure 6

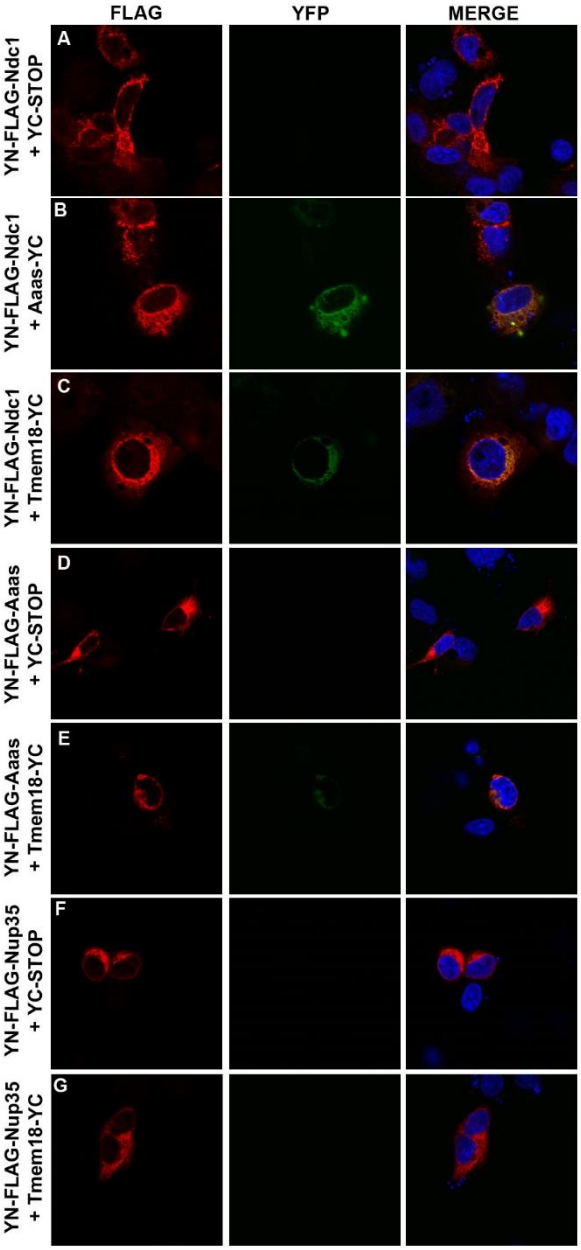
FLAG
YFP
MERGE
A
YN-FLAG-Ndc1 + YC-STOP
B
YN-FLAG-Ndc1 + Aaas-YC
C
YN-FLAG-Ndc1 + Tmem18-YC
D
YN-FLAG-Aaas + YC-STOP
E
YN-FLAG-Aaas + Tmem18-YC
F
YN-FLAG-Nup35 + YC-STOP
G
YN-FLAG-Nup35 + Tmem18-YC

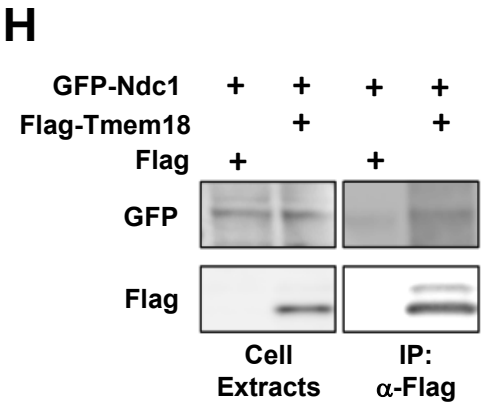
H
GFP-Ndc1 + + + +
Flag-Tmem18 + +
Flag + +
GFP
Flag
Cell Extracts
IP: α-Flag

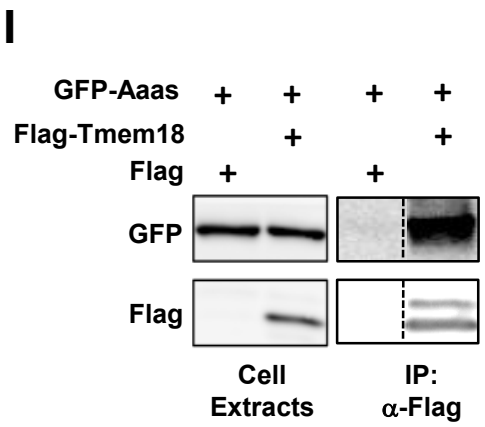
I
GFP-Aaas + + + +
Flag-Tmem18 + +
Flag + +
GFP
Flag
Cell Extracts
IP: α-Flag

The obesity-associated gene *TMEM18* has a role in the central control of appetite and body weight regulation

Larder et al.

SUPPLEMENTARY INFORMATION

SI METHODS

Animals. All procedures were carried out in accordance with guidelines of the United Kingdom Home Office. Animals were kept under controlled temperature (22°C) and a 12-h light, 12-h dark schedule (lights on 7:00–19:00). Standard chow (Special Diet Services, SDS) or a 45% fat diet (D12451, SDS) and water were available *ad libitum*. Mice carrying the knockout first conditional-ready allele *Tmem18*$^{tm1a(EUCOMM)Wtsi}$, abbreviated to Tmem18^{tm1a} in this paper, were generated on a C57BL/6N background as part of the Sanger Mouse Genetics Project (MGP) for the European Conditional Mouse Mutagenesis Program [EUCOMM]. Detailed description of the Sanger Mouse Genetics Project methodology has previously been reported (1-4). Germ line transmission was confirmed by a series of genotyping PCR analyses (http://www.knockoutmouse.org/kb/25/). Following confirmation, mice derived from heterozygous inter cross, were genotyped for the *Tmem18*^{tm1a} allele by PCR. Tmem18$^{flox/flox}$ mice (Tm1c line) were generated by crossing Tmem18^{tm1a} mice to a Flpase deleter line on the same genetic background (5).

Design and Construction of AAV Vectors. To generate a *Tmem18* expressing adeno associated viral (AAV) vector, the cDNA of murine *Tmem18* was cloned into an AAV backbone plasmid under the control of the CMV promoter. AAV vectors expressing GFP under the control of the same promoter were used in a control group of animals as well as to test for optimum titre and accuracy of intranuclear injections in preliminary experiments.

Viral production and purification. AAV vectors were generated by helper virus-free transfection of HEK293 cells using three plasmids. Vectors were purified by two consecutives caesium chloride gradients using an optimized method (6), dialyzed against PBS, filtered, titred by qPCR and stored at -80°C until use. This study used AAV serotype 7.

Stereotactic surgery. Mice were stereotaxically injected with AAV while under isoflurane induced anaesthesia. The coordinates used for the injections were 1.0 mm caudal to bregma, ±0.25 mm lateral to the midline and 5.0 mm below the surface of the skull in all cases. Using a 10µl Hamilton syringe and a 33 gauge needle, 200nl of AAV solution was injected into each side of the hypothalamus over a 1 minute period. After delivery of the virus the needle was left in place for 10 minutes to prevent reflux. The titre of the vector preparations were as follows: AAV7-CMV-GFP $2.1x10^{12}$vg/ml (dose delivered per 200nl $4x10^{7}$vg); AAV7-CMV-Tmem18 $6.3x10^{12}$vg/ml (dose delivered per 200nl $1.2x10^{8}$vg).

Metabolic phenotyping. Body weight measurements were recorded on a weekly basis. Food intake studies were carried out on single housed animals in home cages. Daily food intake was an average taken from 10 consecutive days. Body composition was determined using dual-energy x-ray absorptiometry (DEXA) (Lunar PIXImus2 mouse densitometer, General Electric Medical Systems, Fitchburg, WI). Any animal who did not remain weight stable did not proceed to calorimetry. Energy expenditure was determined using indirect calorimetry in a custom built monitoring system at 20°C (Ideas Studio, Cambridge, UK). Activity was assessed by beam breaks. Beams were 1.25 cm apart and activity measurements were taken to be total beam breaks, rather than consecutive beam breaks. Any data from an animal whose weight changes in the calorimetry system were beyond those seen in the

long-term home cage environment were excluded from analysis. At the end of the experiment animals were sacrificed and tissues collected for further analysis.

Immunohistochemistry and histology. Animals were anesthetized with pentabarbitol (Dolethal) then transcardially perfused with 20 ml PBS followed by 40 ml 10% Formalin/PBS (Sigma). Brains were dissected out and incubated in 15% sucrose/10% Formalin overnight at 4^{o}C. Following cryoprotection in 30% sucrose/PBS, brains were frozen on dry-ice and stored at -80^{o}C overnight. Serial 35 µM sections were taken using a freezing microtome and mounted on glass slides (VWR).

Laser capture microdissection and Q-RT-PCR of fed and 48hr fasted mouse brains. Laser-captured microdissection and total RNA isolation were carried out as previously described (7,8).

Laser capture microdissection and RNA Sequencing of fed and fasted mouse brains. Coronal sections of 20 um thickness were prepared on a cryostat, mounted on RNase-free membrane-coated glass slides with laser microdissection performed using a P.A.L.M. MicrolaserSystem (P.A.L.M. Microlaser Technologies). 2ng of total RNA from each sample was SPIA (single primer isothermal amplification) amplified with an Ovation RNA-Seq System V2 (NuGEN), after which cDNA libraries were prepared using the Encore Rapid DR Multiplex System (NuGEN). Single-end reads (SE50) were sequenced on an Illumina Hi-Seq 2500. Reads were mapped to *Mus Musculus* GRCm38 genome assembly (Ensembl) with Tophat, and comparisons of fasted vs fed samples across the four hypothalamic were performed in RStudio using the edgeR and limma packages.

RNA-Seq analysis of whole hypothalami from wildtype and Tmem18$^{tm1a/tm1a}$ mice. The hypothalamus was dissected from 4 male adult mutant mice and 5 wild-type littermate controls. RNA was extracted using Qiagen RNeasy Mini Kit according to manufacturer's instructions. 1 ug of RNA was used to prepare multiplexed sequencing libraries with an Illumina RNA Library Preparation Kits as per the manufacturer's instructions. Paired end sequencing was performed on the Illumina Hi-Seq 2500, generating 75 bp, stranded paired-end reads. Using STAR (v.2.4)(9) the sequenced reads were aligned to a modified version of the mouse reference genome (GRCm38) with addition of pseudo-chromosomes containing sequences of the knockout first conditional-ready allele (specifically, of the LacZ and neomycin regions of the cassette) for genotyping quality control . The number of reads that mapped to each annotated gene was counted using the HTSeq (v.0.6.1) count function (HTSeq.scripts.count, mode *intersection-nonempty*). The DESeq2 package (v.1.9.29)(10) was used for differential gene expression analysis between mutant and wildtype mice, using the Benjamini-Hochberg procedure (to control for multiple testing, returning an adjusted p value (padj)). A significance cut-off of padj < 0.05 was used.

Quantitative-RT-PCR. Q-RT-PCR was performed on whole hypothalami and brown adipose tissue (BAT). Tissues were dissected from individual mice, snap frozen and stored at -80^{o}C until processed. RNA was extracted using TriSure (Bioline) and reverse transcribed using Il-Prom-II reverse transcription system (Promega) according to manufacturer's instructions. To assess Tmem18 expression within the PVN following surgery micro-punches of the PVN from individual mice were obtained from fresh frozen brains. Accuracy of the micro-punches was confirmed with cresyl violet staining of the cryostat sections after nuclei removal. RNA was isolated from the micro-punch using the Qiagen RNeasy micro system and 50 ng of purified RNA were used in a random-primed first strand cDNA synthesis reaction, using the VILO reverse transcriptase kit (Invitrogen). Quantitative PCR reactions were performed in triplicate on an ABI 7900HT (Applied Biosystems) using ABI PCR master mix and commercially available Taqman probes, according to manufacturer's protocols. All Q-RT-PCR data was normalised to *Gapdh* expression.

Assessment of Targeting Due to the small size of TMEM18 (17kDa) and concerns that the addition of a large protein might impact on expression and function of TMEM18, the AAV-Tmem18 construct did not contain a GFP tag (27 kDa). Therefore, to investigate targeting in the experimental groups, we used both IHC with a TMEM18 antibody (a custom made rabbit polyclonal anti-TMEM18 antibody (Eurogentec, Belgium), 1:500 dilution used in Supplementary Fig 9 B&C), plus PVN punch and Q-RT-PCR (see above). The method of PVN punch and Q-RT-PCR to confirm over-expression within our discrete nuclei gave a numerical value (in this case +1.5 fold increase) that were counted as a 'hit'. If *Tmem18* expression did not reach at least 1.5 fold above baseline (average *Tmem18* expression levels of all GFP injected animals) then they were counted as a 'miss'. Animals that were confirmed as being a 'miss' were removed from our analysis. Of the 19 animals injected with AAV-T18, 4 were used for IHC analysis and Q-RT-PCR expression data were obtained from 14. Of these fourteen, 10 showed increased levels of *Tmem18* expression so were counted as a 'hit' , while 4 did not so were counted as a 'miss'. These four were discarded from further analysis**.** One final animal included in the AAV-T18 group underwent PVN punch with satisfactory cresyl violet staining but insufficient material was generated to quantify mRNA**.** This gave an overall Q-RT-PCR confirmed hit rate of 10/14 (71%). Of the 15 animals injected with AAV-GFP, 4 were used for IHC analysis and Q RT-PCR expression data were obtained from the remaining 11 mice.

Transient transfection and immunocytochemistry. Cos7 cells were plated on four-well glass chamber slides (Nalge Nunc International) at 25,000 cells/ml; 16 h later, each well was transfected with 500 ng of plasmid DNA using Lipofectamine (Thermo Fisher Scientific). After 48 h at 37^{o}C, cells were fixed in 3.7% formaldehyde with either 0.2% TritonX100 for 10 mins at RT or 40 ug/ml Digitonin for 10 mins at 4^{o}C. After washing in PBS, cells were incubated O/N at 4^{o}C with the appropriate primary antibody. The following morning, cells were washed in PBS and incubated with an appropriate secondary antibody conjugated to either a 488 or 594 fluorophore. After washing in PBS, coverslips were mounted using VectaShield hardset mounting media with DAPI (Vector Laboratories) and fluorescent cells detected using a Nikon Eclipse TE2000-U microscope. If colocalization of two proteins was being studied, before mounting with coverslips, cells were incubated with the second primary antibody at RT for 3hrs, washed in PBS then incubated with an appropriate secondary antibody conjugated to either a 488 or 594 fluorophore. Primary antibodies used were as follows: custom made rabbit-anti-mouseTMEM18 antibody raised against amino acids 120-134; Rabbit Polyclonal FLAG tag (Sigma); Monoclonal Anti-FLAG M2 (Sigma), Rabbit-anti-human calnexin (ab22595, Abcam); Goat-anti-mouse lamin B (Santa Cruz Biotech, sc-6217) and Rabbit polyclonal Myc tag (Abcam, ab9106).

Pulldown and Mass Spec analysis. HEK293 cells were cultured in Dulbecco's Modified Minimal Essential Medium (DMEM) supplemented with 10% FCS at 37oC under 5% CO2. For protein over expression studies, transient transfection in HEK293 cells was performed using a CalPhos kit according to the manufacturer's protocol. 48 hours post transfection, cells were harvested and Flag immunoprecipitations (IPs) were performed from the resulting lysates as described (11). For MS analysis, Flag immunoprecipitates were subjected to SDS-PAGE, each lane was excised and cut into 6 chunks with the proteins digested in-gel using trypsin. The resulting tryptic peptides were eluted and analysed by LC-MSMS using an LTQ-OrbiTrap XL (Thermo) coupled to a nanoAcquity (Waters) in a top 6 DDA fashion. Raw files were processed using MaxQuant 1.3.0.5. Searches were performed using the Andromeda search engine against a Uniprot Mus musculus database (downloaded 14/08/12). Oxidation (M), acetylation (protein N-terminus) and deamidation (NQ) were set as variable modifications. Data was filtered to a peptide and protein FDR of 0.01. Validation of MS analysis results was performed as previously described (11).

Direct and Competitive Bimolecular Fluorescence Complementation. YFP constructs and controls were a kind gift from David Savage (12). Interactions between YN-FLAG-NDC1/AAAS/NUP35 and MYC-TMEM18-YC in COS-7 cells were assessed by transfecting 200 ng of each YN construct with 200 ng of each YC construct. Four hours post transfection, cells were incubated at 32°C for 20hr and 30°C for 2.5hr to promote the formation of YFP. Twenty-four hours post transfection, cells were fixed, permeabilized, and stained with anti-FLAG mouse monoclonal antibody (Sigma) followed by goat anti-mouse Alexa 594 secondary antibody (Abcam).

Bioinformatic Analysis. TMEM18 orthologues (144 sequences) from OMA database (http://omabrowser.org) were aligned with Muscle (13) and submitted to HHpred searches (14) in all available microbial fungal and metazoan protein databases and collections of HMM profiles using MPI Toolkit suite(15). The homology models were based on the HHpred alignments. The structures were displayed and examined with Protein Workshop Viewer (16).

SI- SUPPLEMENTARY REFERENCES

1.Skarnes WC, Rosen B, West AP, Koutsourakis M, Bushell W, Iyer V, Mujica AO, Thomas M, Harrow J, Cox T, et al. A conditional knockout resource for the genome-wide study of mouse gene function. Nature. 2011;474(7351):337-42.

2.Bradley A, Anastassiadis K, Ayadi A, Battey JF, Bell C, Birling MC, Bottomley J, Brown SD, Burger A, Bult CJ, et al. The mammalian gene function resource: the International Knockout Mouse Consortium. Mammalian genome : official journal of the International Mammalian Genome Society. 2012;23(9-10):580-6.

3.Pettitt SJ, Liang Q, Rairdan XY, Moran JL, Prosser HM, Beier DR, Lloyd KC, Bradley A, and Skarnes WC. Agouti C57BL/6N embryonic stem cells for mouse genetic resources. Nature methods. 2009;6(7):493-5.

4.White JK, Gerdin AK, Karp NA, Ryder E, Buljan M, Bussell JN, Salisbury J, Clare S, Ingham NJ, Podrini C, et al. Genome-wide generation and systematic phenotyping of knockout mice reveals new roles for many genes. Cell. 2013;154(2):452-64.

5.Kranz A, Fu J, Duerschke K, Weidlich S, Naumann R, Stewart AF, and Anastassiadis K. An improved Flp deleter mouse in C57Bl/6 based on Flpo recombinase. Genesis. 2010;48(8):512-20.

6.Ayuso E, Mingozzi F, and Bosch F. Production, purification and characterization of adeno-associated vectors. Curr Gene Ther. 2010;10(6):423-36.

7.Tung YC, Ma M, Piper S, Coll A, O'Rahilly S, and Yeo GS. Novel leptin-regulated genes revealed by transcriptional profiling of the hypothalamic paraventricular nucleus. J Neurosci. 2008;28(47):12419-26.

8.Jovanovic Z, Tung YC, Lam BY, O'Rahilly S, and Yeo GS. Identification of the global transcriptomic response of the hypothalamic arcuate nucleus to fasting and leptin. J Neuroendocrinol. 2010;22(8):915-25.

9.Dobin A, Davis CA, Schlesinger F, Drenkow J, Zaleski C, Jha S, Batut P, Chaisson M, and Gingeras TR. STAR: ultrafast universal RNA-seq aligner. Bioinformatics. 2013;29(1):15-21.

10.Love MI, Huber W, and Anders S. Moderated estimation of fold change and dispersion for RNA-seq data with DESeq2. Genome Biol. 2014;15(12):550.

11.Gulati P, Cheung MK, Antrobus R, Church CD, Harding HP, Tung YC, Rimmington D, Ma M, Ron D, Lehner PJ, et al. Role for the obesity-related FTO gene in the cellular sensing of amino acids. Proc Natl Acad Sci U S A. 2013;110(7):2557-62.

12.Gandotra S, Lim K, Girousse A, Saudek V, O'Rahilly S, and Savage DB. Human frame shift mutations affecting the carboxyl terminus of perilipin increase lipolysis by failing to sequester the adipose triglyceride lipase (ATGL) coactivator AB-hydrolase-containing 5 (ABHD5). The Journal of biological chemistry. 2011;286(40):34998-5006.

13.Edgar RC. MUSCLE: multiple sequence alignment with high accuracy and high throughput. Nucleic Acids Res. 2004;32(5):1792-7.

14. Soding J. Protein homology detection by HMM-HMM comparison. Bioinformatics. 2005;21(7):951-60.

15. Alva V, Nam SZ, Soding J, and Lupas AN. The MPI bioinformatics Toolkit as an integrative platform for advanced protein sequence and structure analysis. Nucleic Acids Res. 2016;44(W1):W410-5.

16.Moreland JL, Gramada A, Buzko OV, Zhang Q, and Bourne PE. The Molecular Biology Toolkit (MBT): a modular platform for developing molecular visualization applications. BMC Bioinformatics. 2005;6(21.

The obesity-associated gene *TMEM18* has a role in the central control of appetite and body weight regulation

Larder et al.

SUPPLEMENTARY INFORMATION

SI figures

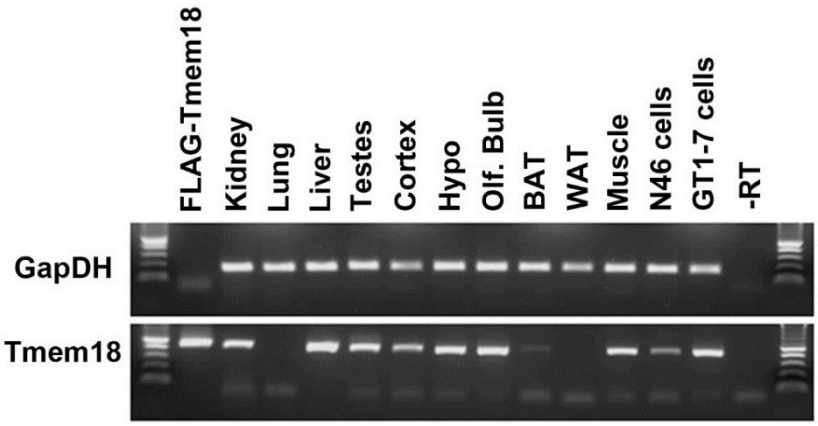

Fig S1. Analysis of *Tmem18* expression. RT-PCR analysis of *Tmem18* expression in various mouse tissues. GapDH was used as a positive control.

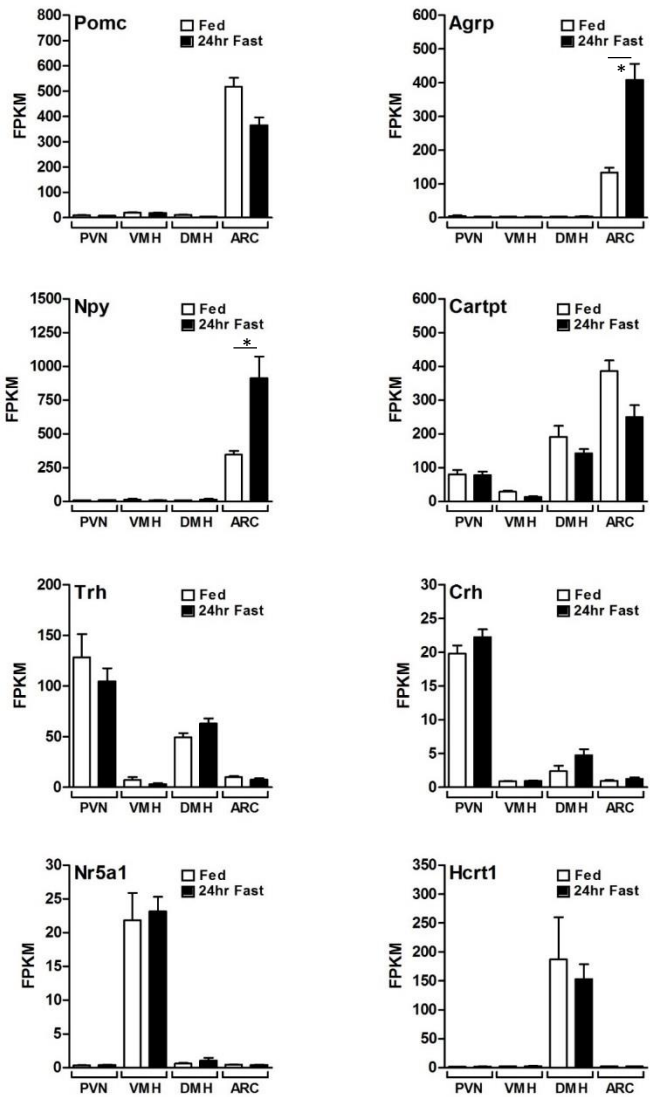

Fig. S2. Validation of laser-capture microdissection specificity in *ad libitum fed* and 24hr fasted wildtype mice. Bar charts showing FPKM values for genes known to be enriched in given hypothalamic nuclei. White bars show fed mice, black bars show mice fasted for 24hrs. *Pomc*, *Agrp*, *Npy*, *Crh*, *Nr5a1*, and *Hcrt* have expression specific to their corresponding hypothalamic region (FDR<0.001). Upregulation of expression with fasting is evident in the arcuate nucleus for *Agrp* (FDR = 0.001) and *Npy* (FDR = 0.017). PVN, paraventricular nucleus; VMH, ventral medial hypothalamus; DMH, dorsal medial hypothalamus; ARC, arcuate nucleus, *Pomc*, pro-opiomelanocortin; *Agrp*, agouti-related peptide; *Cartpt*, cocaine and amphetamine-regulated transcript protein; *Trh*, thyrotropin releasing hormone; *Crh*, corticotropin releasing hormone; *Nr5a1*, nuclear receptor subfamily 5 group A member 1; Hcrt, hypocretin neuropeptide precursor.

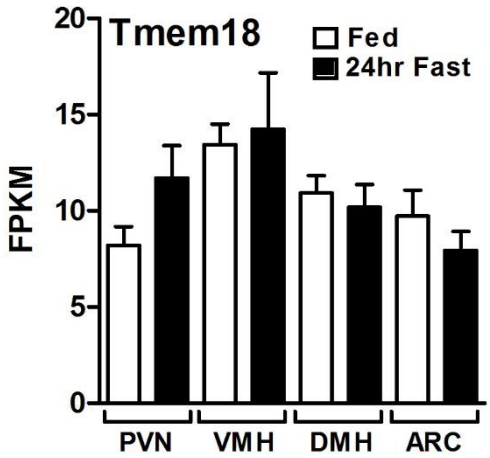

Fig S3. Gene expression of *Tmem18* in laser captured hypothalamic nuclei from *ad libitum* fed and 24 hour fasted wildtype mice. White bars show fed mice, black bars show mice fasted for 24hrs. PVN, paraventricular nucleus; VMH, ventral medial hypothalamus; DMH, dorsal medial hypothalamus; ARC, arcuate nucleus. No significant difference between fed vs fast in any nuclei.

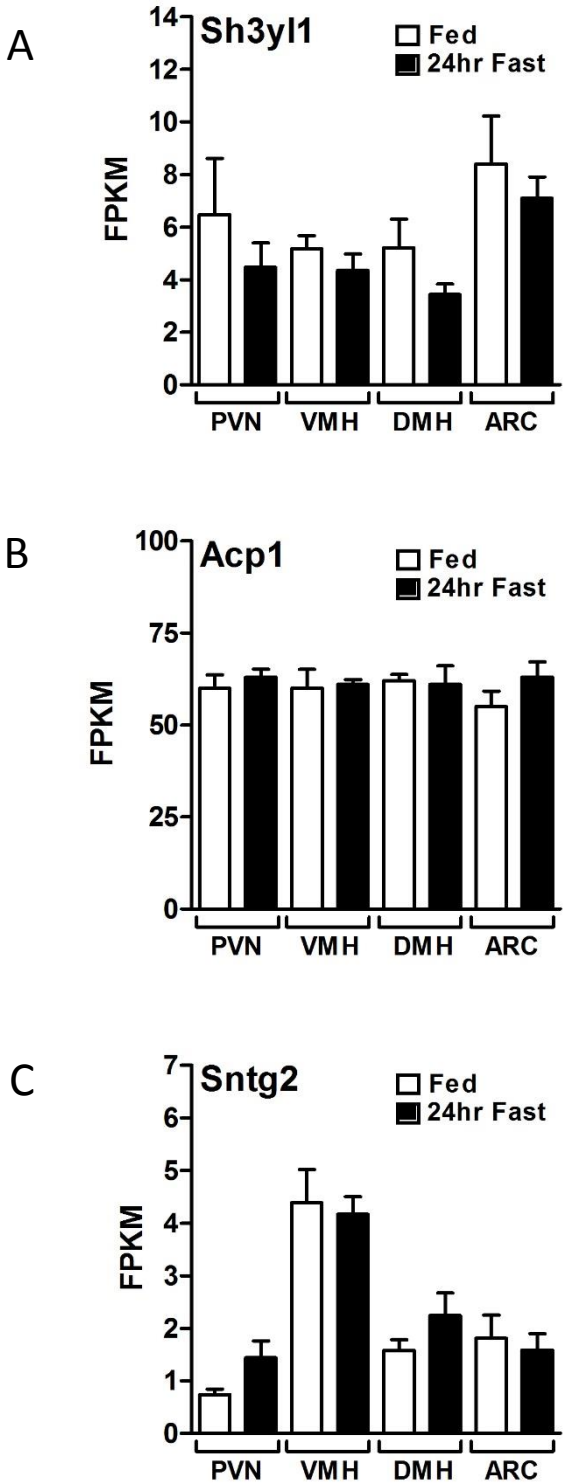

Fig S4. Expression of genes neighbouring *Tmem18* in laser captured hypothalamic nuclei from ad libitum fed and 24 hour fasted wildtype mice. (A) *Sh3yl1*, **(B)** *Acp1*, **(C)** *Sntg2*. White bars show fed mice, black bars show mice fasted for 24hrs. PVN, paraventricular nucleus; VMH, ventral medial hypothalamus; DMH, dorsal medial hypothalamus; ARC, arcuate nucleus. For each gene, no significant difference between fed vs fast in any nuclei.

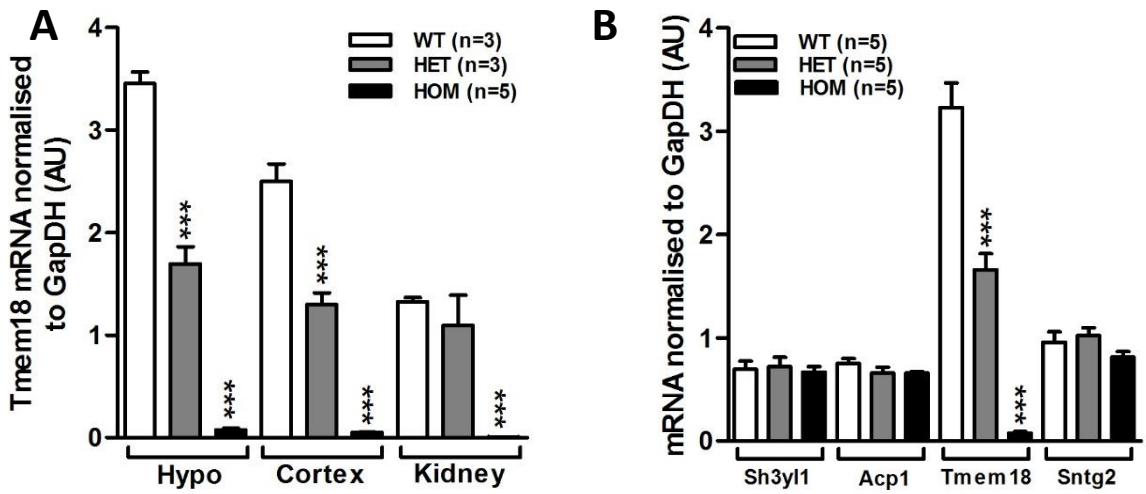

Fig S5. Validation of the *Tmem18tm1a* model. (A) Gene expression of *Tmem18* in the hypothalamus, cortex and kidney of WT (white bars), heterozygous (grey bars) and homozygous (black bars) mice, normalised to expression of GAPDH. **(B)** Gene expression of *Tmem18* and its neighbouring genes *Sh3yl1*, *Acp1* and *Sntg2* in the hypothalamus of WT, heterozygous and homozygous mice, normalised to expression of *Gapdh*. Data are expressed as mean ± SEM *** $p<0.001$ vs WT mice.

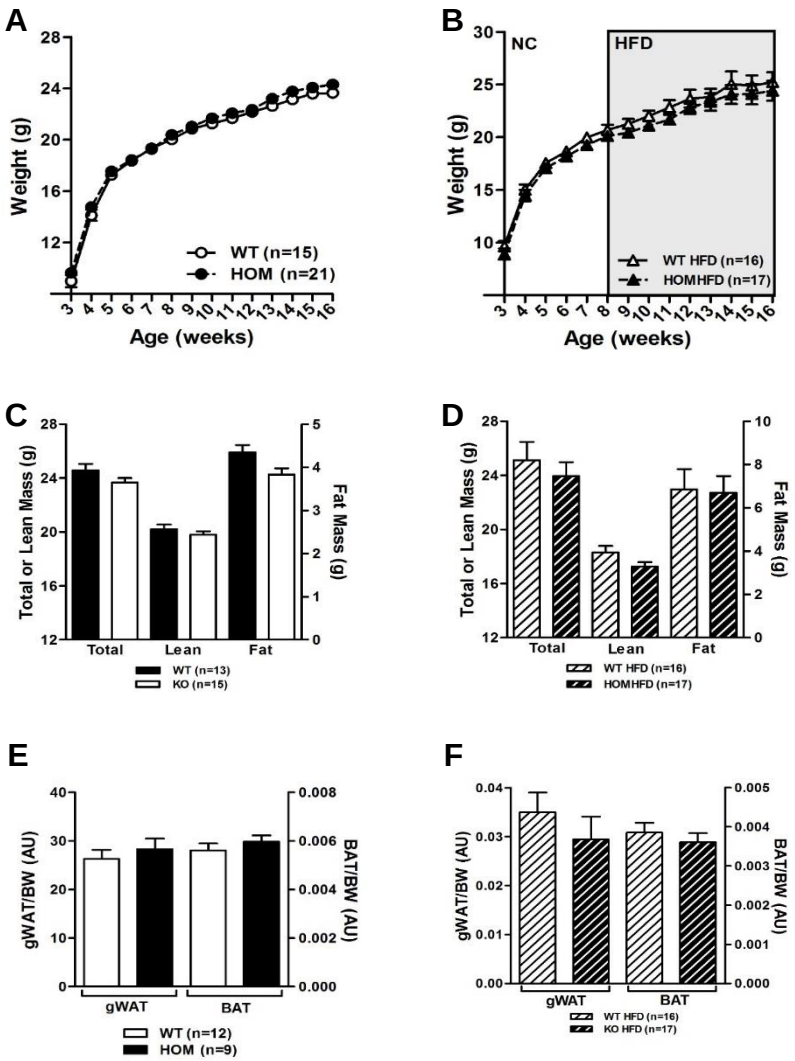

Fig S6. Effect of loss of expression of *Tmem18* on body weight, length and composition in female mice maintained either on a normal chow diet or 45% HFD. (A) Body weights of *Tmem18*$^{wt/wt}$ (WT) and *Tmem18*$^{tm1a/tm1a}$ (HOM) female mice on normal chow. **(B)** Body weights of WT and HOM female mice placed on a high fat diet (HFD) at 8 weeks of age. **(C)** Body composition analyses showing total, lean or fat mass of 14-week old WT and HOM female mice on normal chow. **(D)** Body composition analyses showing total, lean or fat mass of 14-week old WT and HOM female mice placed on HFD at 8 weeks of age. **(E)** Weights of gonadal white adipose tissue (gWAT) and brown adipose tissue (BAT) of WT and homozygous mice at 18 weeks of age, normalised to body weight. **(F)** Weights of gonadal white adipose tissue (gWAT) and brown adipose tissue (BAT) of 18-22 week old WT and homozygous mice fed a HFD from 8 weeks of age normalised to body weight. Data are expressed as mean ± SEM. WT mice are represented by white symbols and bars. HOM mice are represented by black symbols and bars. Time-course data were analysed using the repeated measures ANOVA model. p-values for C-F were calculated using a two-tailed distribution unpaired Student's t-test . No significant differences were seen between genotypes in any comparison.

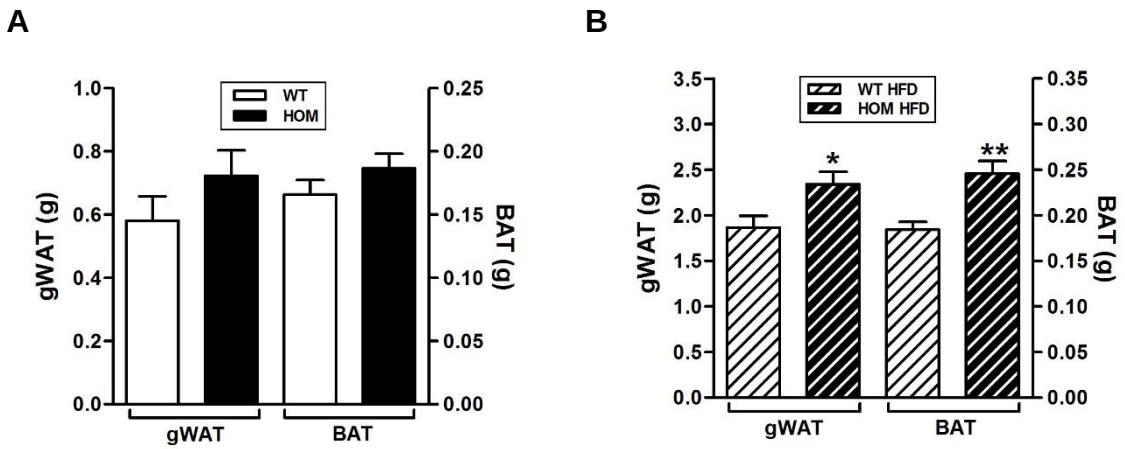

Fig S7 . Effect of loss of expression of *Tmem18* on regional fat mass (A) Weights of gonadal white adipose tissue (gWAT) and brown adipose tissue (BAT) of WT and homozygous mice at 18 weeks of age (WT, n=12; HOM, n=9). **(B)** Weights of gonadal white adipose tissue (gWAT) and brown adipose tissue (BAT) of 18-22 week old WT and homozygous mice fed a HFD from 8 weeks of age (WT, n=15; HOM, n=20). Data are expressed as mean ± SEM. * $p<0.05$, ** $p<0.01$ vs WT mice.

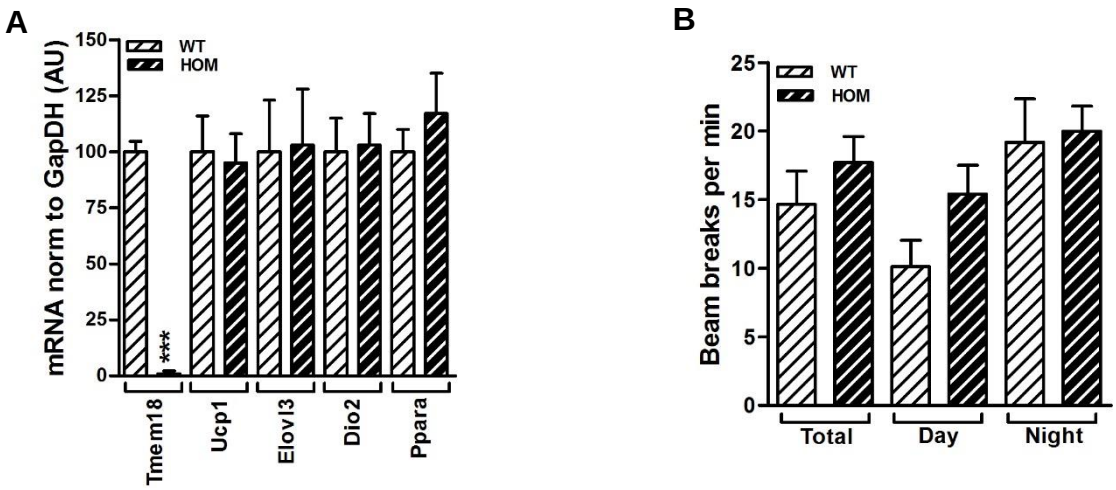

Fig S8. Effect of loss of expression of *Tmem18* on BAT and activity levels and food intake in male mice fed a HFD. (A) Q-RT-PCR analysis of *Tmem18* and brown adipose tissue (BAT) markers *Ucp1*, *Elovl3* and *Ppara* expression in WT and HOM male mice (WT, n=7; HOM, n=5). **(B)** Activity of WT and HOM mice during indirect calorimetry experiment represented by beam breaks per minute during total time in cage, the day and at night (WT, n=13; HOM, n=18). Data are expressed as mean ± SEM. *** $p<0.001$ vs WT mice.

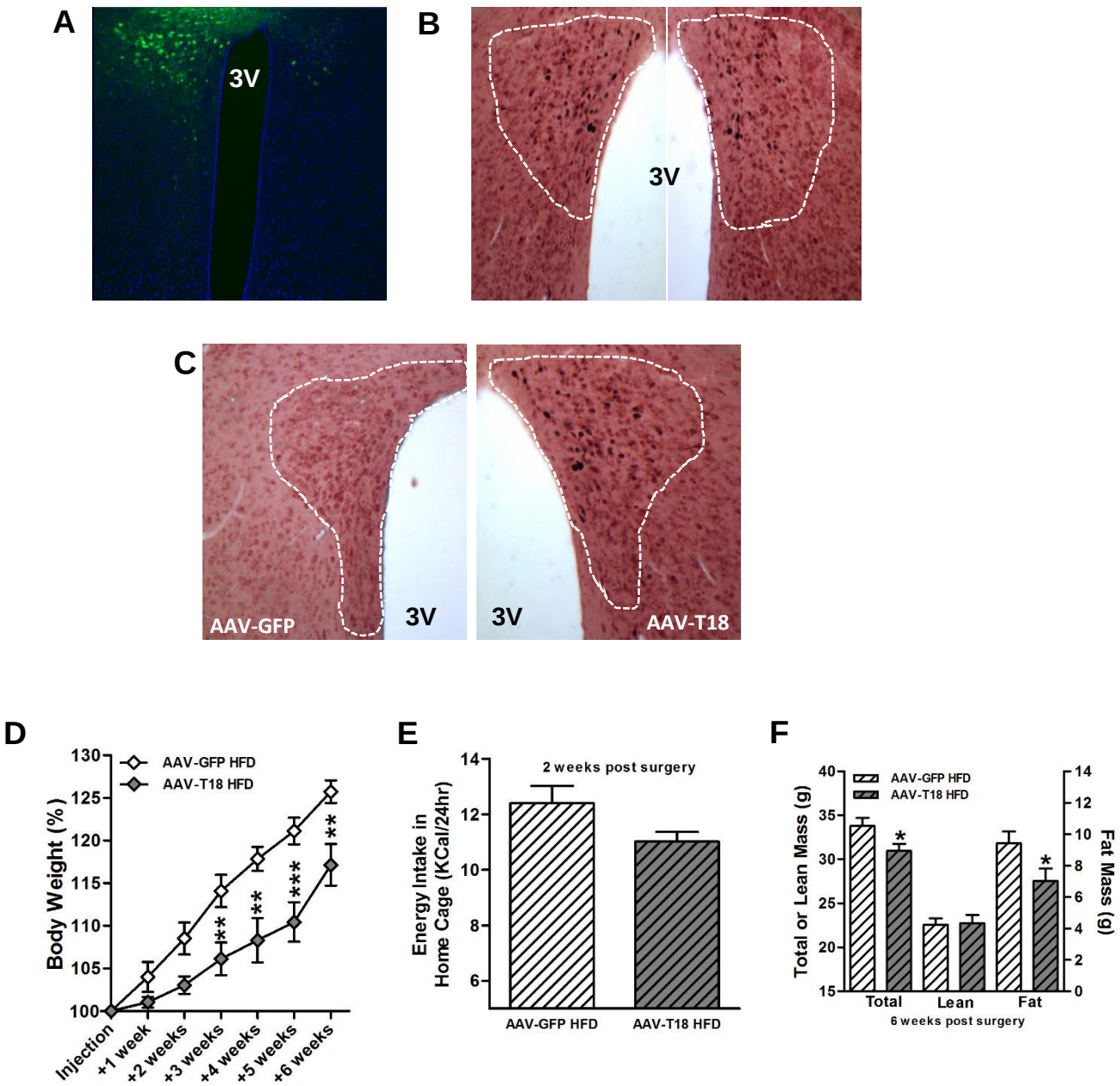

Fig S9. Overexpression of *Tmem18* within the PVN. (A) Representative section showing discrete GFP expression (green) within the PVN two weeks after unilateral AAV-GFP injection, with DAPI staining shown in blue. 3V, 3rd ventricle.**(B)** Representative section showing IHC to confirm discrete TMEM18 expression within the PVN two weeks after bilateral AAV-T18 injection. **(C)** Representative sections showing IHC to detect TMEM18 protein expression within the PVN after injection of either AAV-GFP (left) or AAV-T18 (right). **(D)** Percentage change in body weight of mice placed on a high fat diet immediately after surgery and measured weekly for 6 weeks after bi-lateral PVN injections with either an AAV-T18 cDNA or AAV-GFP (n= 6 each group). **(E)** Average 24-hour energy intake of mice on HFD, measured in their home cage, 2 weeks post-surgery (n= 6 each group). **(F)** Body composition analyses of mice on HFD showing total, lean or fat mass at 6 weeks post surgery (n= 6 each group. Data are expressed as mean ± SEM, * $p<0.05$, ** $p<0.01$, *** $p<0.001$ vs GFP injected mice.

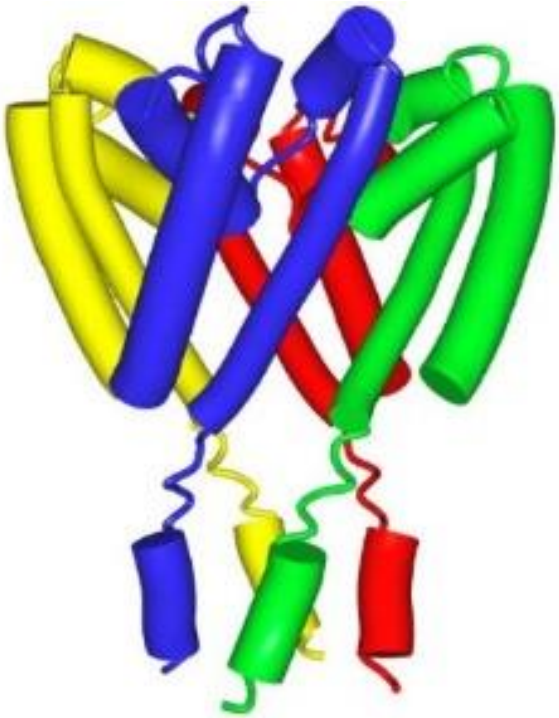

Fig S10. Tentative illustrative sketch of TMEM18 modelled as a tetramer. The individual monomers are displayed in different colours. The conserved C-terminus (~25 amino acids) is exposed to the cytoplasm and the upper four-helix domain is embedded in the membrane with its N-terminus pointing to the cytoplasm. The preceding sequence of ~50 amino acids is exposed to the cytoplasm but cannot be modelled due to the lack of homology.

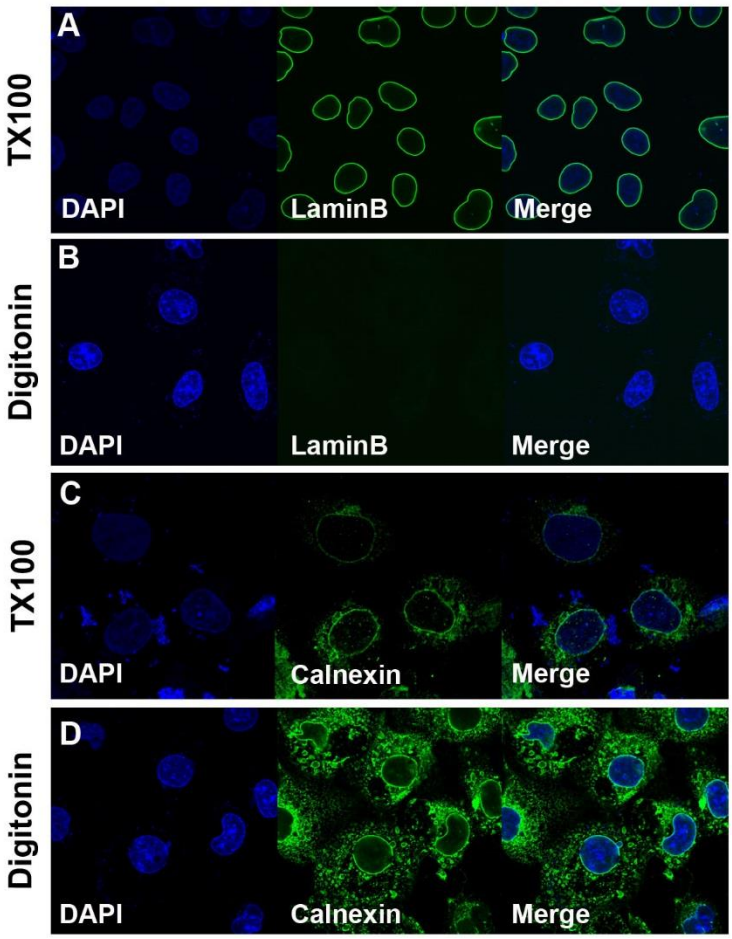

Fig S11. Over-expression of N-terminal FLAG-tagged TMEM18 in COS cells treated with either TX-100 (permeabilises both plasma & nuclear membrane) or digitonin (permeabilises plasma membrane only). Lamin **(A&B)** and Calnexin **(C&D)** are shown as controls.

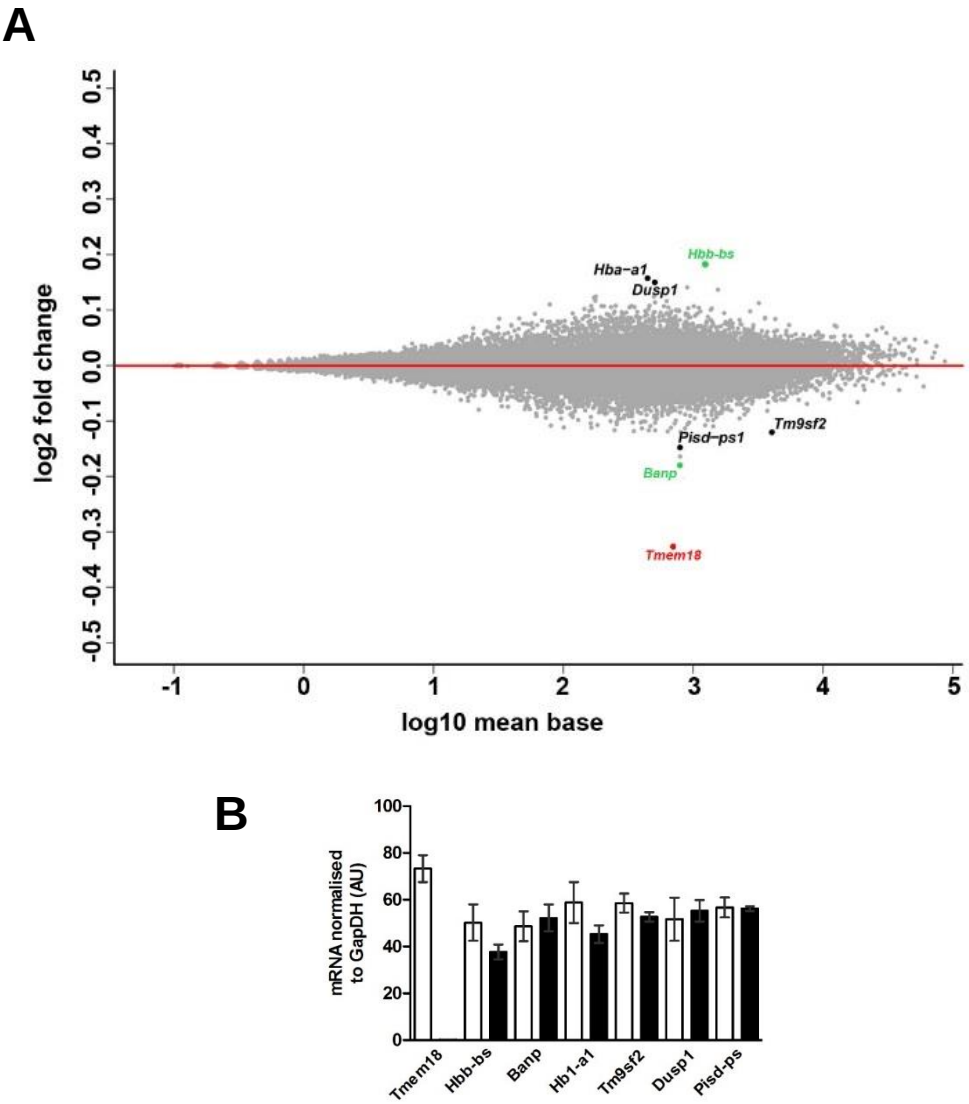

Fig S12. Effect of loss of *Tmem18* on the hypothalamic transcriptome. (A) MA plot showing differentially expressed genes in the hypothalami of *Tmem18*$^{wt/wt}$ and *Tmem18*$^{tm1a/tm1a}$ male mice. *Tmem18*, the only gene with a statistically significant difference in expression, is shown in red. The next two transcripts with the largest difference in expression (*Hbb-bs* and *Banp*) are shown in green. Four additional genes selected for confirmatory analysis are shown in black. **(B)** Q-RT-PCR analysis of selected genes in the hypothalami of *Tmem18*$^{wt/wt}$ and *Tmem18*$^{tm1a/tm1a}$ male mice.

Supplementary Table 1;List of proteins identified in cells expressing FLAG tagged TMEM18 by immunoprecipitation using FLAG antibody.